Meteoritics & Planetary Science 39, Nr 3, 425–451 (2004)
Abstract available online at http://meteoritics.org

Geology, petrography, shock petrography, and geochemistry of impactites and target rocks from the Kärdla crater, Estonia

V. PUURA,[1]* H. HUBER,[2†] J. KIRS,[1] A. KÄRKI,[3] K. SUUROJA,[4] K. KIRSIMÄE,[1] J. KIVISILLA,[4] A. KLEESMENT,[5] M. KONSA,[5] U. PREEDEN,[1] S. SUUROJA,[5] and C. KOEBERL[2]

[1]Institute of Geology, University of Tartu, Vanemuise street 46, 51014 Tartu, Estonia
[2]Department of Geological Sciences, University of Vienna, Althanstrasse 14, A-1090 Vienna, Austria
[3]Institute of Geosciences, University of Oulu, Box 3000, FIN-90401 Oulu, Finland
[4]Geological Survey of Estonia, Kadaka tee 80/82, 12618 Tallinn, Estonia
[5]Institute of Geology, Tallinn Technical University, Estonia pst. 7, 10143 Tallinn, Estonia
[†]Present address: Institute of Geophysics and Planetary Physics, University of California Los Angeles, 595 Charles Young Drive, Los Angeles, California 90095, USA
*Corresponding author. E-mail: vaino.puura@ut.ee

(Received 20 December 2002; revision accepted 7 January 2004)

Abstract–The Kärdla crater is a 4 km-wide impact structure of Late Ordovician age located on Hiiumaa Island, Estonia. The 455 Ma-old buried crater was formed in shallow seawater in Precambrian crystalline target rocks that were covered with sedimentary rocks. Basement and breccia samples from 13 drill cores were studied mineralogically, petrographically, and geochemically. Geochemical analyses of major and trace elements were performed on 90 samples from allochthonous breccias, sub-crater and surrounding basement rocks. The breccia units do not include any melt rocks or suevites. The remarkably poorly mixed sedimentary and crystalline rocks were deposited separately within the allochthonous breccia suites of the crater. The most intensely shock-metamorphosed allochthonous granitoid crystalline-derived breccia layers contain planar deformation features (PDFs) in quartz, indicating shock pressures of 20–35 GPa. An apparent K-enrichment and Ca-Na-depletion of feldspar- and hornblende-bearing rocks in the allochthonous breccia units and sub-crater basement is interpreted to be the result of early stage alteration in an impact-induced hydrothermal system. The chemical composition of the breccias shows no definite sign of an extraterrestrial contamination. By modeling of the different breccia units with HMX-mixing, the indigenous component was determined. From the abundances of the siderophile elements (Cr, Co, Ni, Ir, and Au) in the breccia samples, no unambiguous evidence for the incorporation of a meteoritic component above about 0.1 wt% chondrite-equivalent was found.

INTRODUCTION

In the Baltic Sea region, 15 meteorite impact structures of Paleozoic age have been identified to date (Abels et al. 2002). During the Paleozoic era, the Baltic area developed as a large and shallow epi-continental sea or flat sedimentary lowland. At the end of the Paleozoic era, a thin (mostly <500 m, maximum ~3-km-thick) sequence of unconsolidated sediments covered the Precambrian basement. From the late Paleozoic era and during the Meso-Cenozoic era, the present Fennoscandian Shield was re-exposed due to uplift and erosion. Consequently, in the Paleozoic era, asteroids or comets hit a two-layered target either in marine or continental environments, depending on high or low sea levels. Among these 15 impact craters (see Fig. 1), six structures of Middle to Late Ordovician (450–470 Ma) age form a prominent group, i.e., Granby, Hummeln, Karikkoselkä, Lockne, Tvären, and Kärdla. The majority of them formed in a marine environment (Puura et al. 1994; Abels et al. 2002). Kärdla is the best-preserved crater among the Paleozoic marine impact structures in this region. The Kärdla crater formed during the early Late Ordovician (see IUGS 2000) and has been dated at 455 Ma (Puura et al. 1989; Puura and Suuroja 1992) based on the stratigraphic position of the Kärdla distal ejecta in the sequence of the Caradoc Series.

Kärdla is also a good target for the study of unmelted suites of impactites produced in marine environments and combined sedimentary-crystalline targets. Impactites from

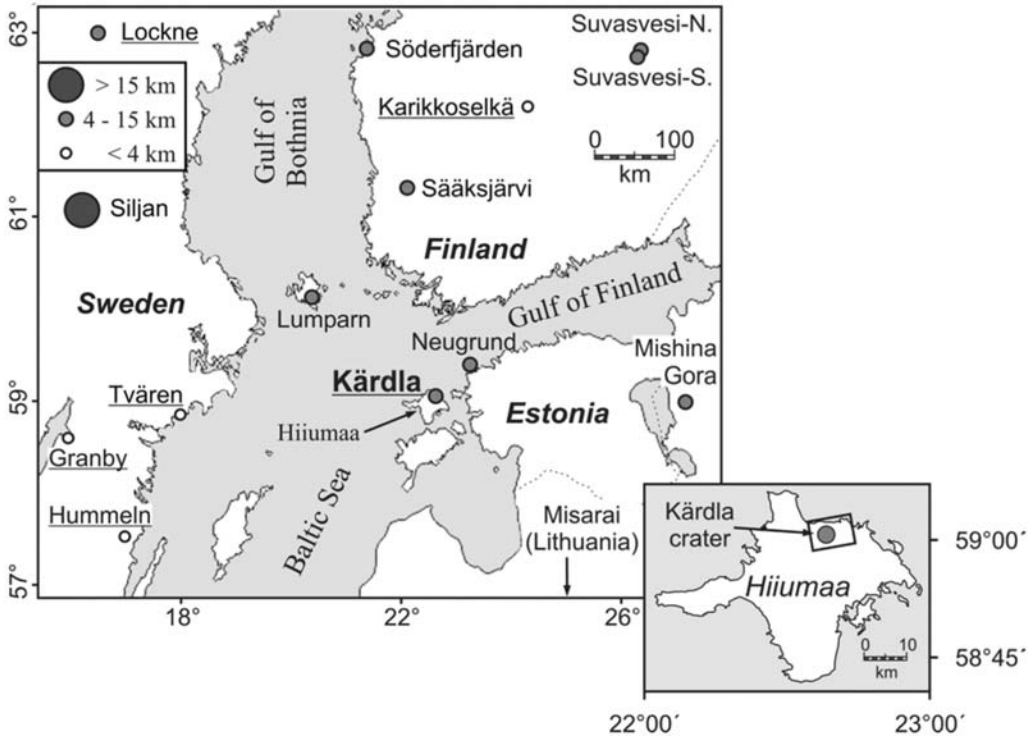

Fig. 1. Geographic map of the 15 known Paleozoic impact structures in the Baltic Sea region. Among others, the Kärdla crater in Estonia belongs to the Middle to Late Ordovician age group, the most common in this region. The location of the Kärdla crater (lat. 58°59´N, long. 22°46´E) on Hiiumaa Island is shown in the close-up. The rectangle in the insert indicates the part shown in the geological map (Fig. 2).

the Kärdla crater, both allochthonous crater-fill and autochthonous sub-crater rocks, are of silicate-dominated composition.

During impact-induced processes, these rocks were enriched in potassium and depleted in sodium and calcium (Puura and Suuroja 1992; Puura et al. 2000a, b). The dominant type of alteration is metasomatic replacement of the rock-forming feldspars, hornblende, and biotite with secondary minerals. The occurrence and mechanisms of large-scale K-metasomatism in impact structures remain poorly studied. At many craters, fissures, vugs, and pores in impactites are filled with Ca- and Na-rich minerals, as described for the Manson crater in the USA (McCarville and Crossey 1996) or the Popigai, Kara, and Puchezh-Katunki craters in Russia (Naumov 1999, 2002; Masaitis et al. 2004). These secondary minerals include zeolites, clay minerals, and carbonates. However, at Kärdla, veins and vugs filled with the Ca-Mg-rich minerals calcite, dolomite, and chlorite are only a considerably small admixture in K-enriched impactites.

Drilling of the Kärdla crater was performed by the Geological Survey of Estonia at 30 different sites with maximum depths of 800 m, but most cores penetrated to an average depth of 300 m (Suuroja 1996; Puura and Suuroja 1992). The studied samples are from 13 of these drill cores (for locations, see Figs. 2 and 3) that penetrated between 79.7 and 815.2 m into the crater-fill deposits and sub-crater basement in the crater moat, central uplift, crater rim, and ejecta layer outside the crater proper. Core K1 was drilled in 1989–1990 in impactites with diameters of 60 and 40 mm down to 815.2 m, and core K18 was drilled in 1984 with a diameter of 60 mm to a depth of 431.4 m. Both cores are stored at the Arbavere field station of the Geological Survey of Estonia. Short descriptions of these two cores, including core logs, were given by Suuroja (1996) and in unpublished reports of the Geological Survey of Estonia. A detailed description of core K1 is given by Suuroja et al. (2002b). Puura and Suuroja (1992) published preliminary data on chemical and mineralogical changes of Precambrian basement silicate target rocks.

The aim of the present paper is to present results of systematic studies of impact lithologies and target rocks of the Kärdla crater. The research focused on the geochemical-mineralogical composition and metasomatic alteration, on the spatial distribution of shocked minerals, and on the mixing of target rocks and the admixture of a meteoritic component.

GEOLOGICAL SETTING OF THE CRATER AND IMPACT LITHOLOGIES

The Multilayer Target

The buried crater structure is located in the northwestern marginal part of the Russian platform, within the exposure of the Upper Ordovician and Lower Silurian. The crater site is

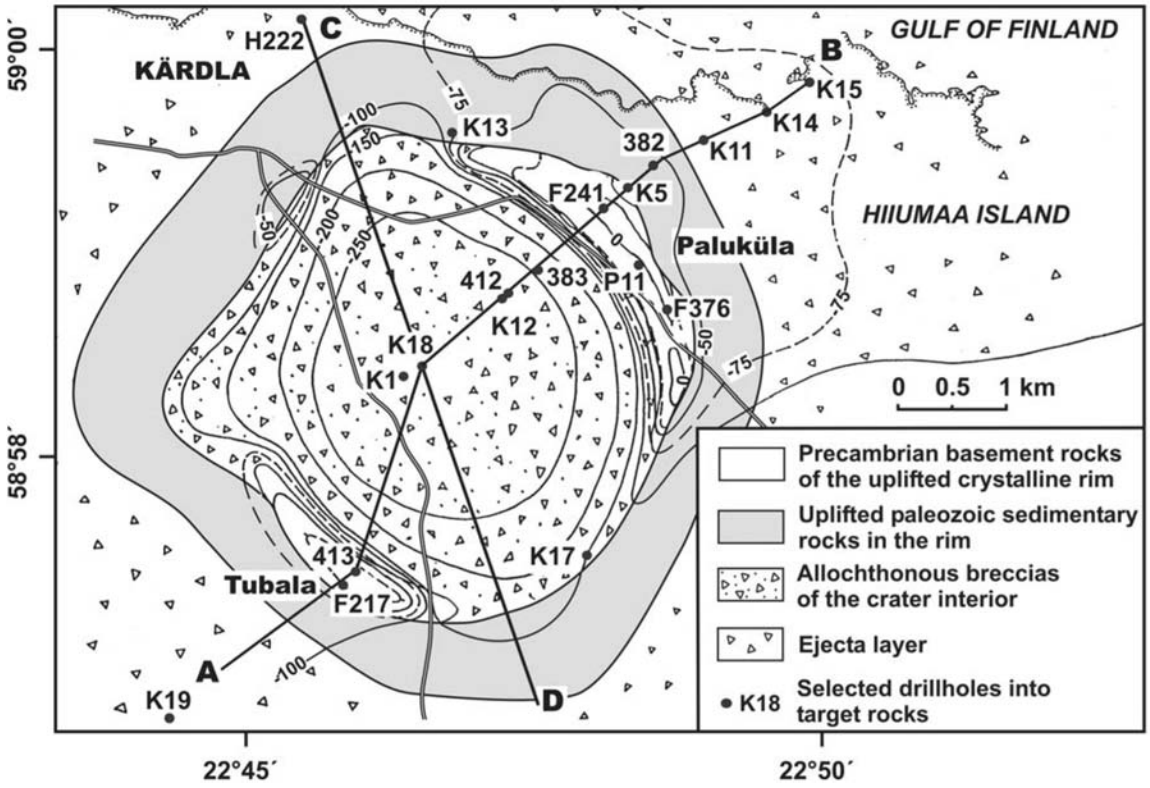

Fig. 2. Subsurface geological map of the Kärdla crater. Post-impact formations are removed, and contour lines show the subsurface topography of target rocks and impact breccias that underlie the post-impact cover-rocks. The Paleozoic rocks in the rim area are mainly Cambrian sandstones and claystones. Cross sections AB and CD are shown in Fig. 3.

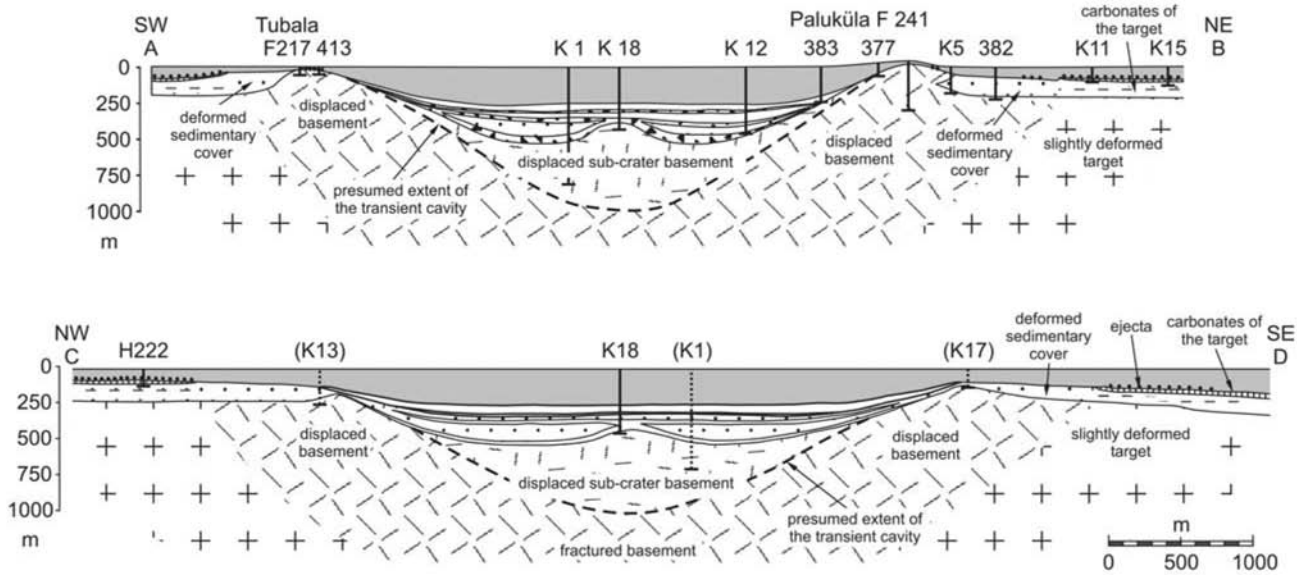

Fig. 3. Generalized cross sections of the Kärdla crater. Top: SW-NE section across the uplifted crystalline basement in the rim (drill cores at Paluküla and Tubala). Bottom: NW-SE section through the gullies in the rim. The locations of the cross sections are shown in Fig. 2 (AB, CD). Post-impact cover sediments are shown in gray. Logs of the allochthonous breccias of boreholes K1 and K18 are given in Figs. 4a–4c. For the subsurface geology below the cover, see Fig. 2.

on Hiiumaa Island, Estonia, in a flat, low, near-shore area. Only low hills with up to 23 m elevation mark the most elevated buried fragments of the crystalline rim (e.g., the Paluküla and Tubala hills; see Fig. 2). A flat wetland corresponds to the crater proper.

At present, the composite lithologies of the Kärdla area consist of 170 m-thick uppermost Middle Ordovician to Cambrian and uppermost Vendian (Neoproterozoic III, after IUGS 2000) sedimentary rocks underlain by Paleoproterozoic (Svecofennian, 1.9–1.8 Ga) crystalline basement (see Fig. 3). The sea at the impact site was a shallow-water, near-shore zone of the Paleo-Baltic basin, which opened to the Iapetus Ocean far in the southwest. The lower Paleozoic sedimentary cover and Paleoproterozoic crystalline basement were both affected by the impact. At the time of the impact event, the target consisted of three principal layers (from the top):

1. Seawater, less than 100 m yet probably only 20–50 m deep (Puura and Suuroja 1992);
2. Sediments, estimated thickness ~200 m;
3. The crystalline basement.

The sedimentary cover consisted of (from the top):

1. Limestones and clayish limestones with an admixture of goethite-rich oolites and glauconite grains in its lowermost layers, 25 m;
2. Organic-rich (metalliferous) mud (presently, black shale), weakly consolidated, ~2 m;
3. Quartz silts with clay inter-layers and sands, weakly consolidated, ~170 m.

The crystalline basement consisted of the upper (5–25 m) weathered (usually kaolinite-rich) and lower fresh parts, with a gradual transition between the two. The basement is composed of igneous, mainly migmatitic granite, and metamorphic (amphibolites and granitoid gneisses) rocks (Koppelmaa et al. 1996). Microcline-plagioclase granites form veins and more massive bodies. Metamorphic rocks in the surroundings of the Kärdla crater contain migmatized biotite or biotite-amphibole gneisses, biotite-amphibole-plagioclase amphibolites, and quartzites. For the characterization of impact-affected rocks and mixing calculations, the chemical composition of pre-impact rocks were used from Koppelmaa et al. (1996) and Kivisilla et al. (1999).

The Impact Structure and Its Post-Impact History

The sub-surface map of the crater (without post-impact deposits; see Fig. 2) and the cross sections (Fig. 3) show the structure of the crater. To restore the possible morphology of the transient cavity at Kärdla, we can compare it to the Brent crater, Canada (B. A. Ivanov 2000, personal communication). For the present study, we calculated approximate volumes in km^3 as follows (Figs. 2–4): transient cavity (8 km^3), present crater below the target surface (2.3), uplifted (displaced) sub-crater basement (3.5), excavated rocks (3.5) (including: sedimentary cover [2.3] and crystalline basement [1.2]), and allochthonous breccias within the crater (0.5) (including: sediment-dominated [0.3] and crystalline [0.2]). For the calculations, the vertical parabolic cross section of the crater was divided into truncated cones considering the thickness of target layers in the volume of the transient cavity and impact-stratigraphic units in the present crater. The morphology of breccia units and the proportions of sedimentary to crystalline rocks in the impact breccia units were estimated from logs of cores K1, K18, and K12. The results of the calculations were rounded to the nearest 0.1 km^3.

The crater rim wall consists of four horseshoe-shaped elevated parts, including Paluküla High in the east-northeast and Tubala in the west-southwest. The crest of the wall segments was eroded deeply enough to expose the crystalline core before the final burial under post-impact sediments. In the gullies (compare profiles in Fig. 2), the post-impact breccia layer overlies deformed Cambrian sedimentary rocks. The amount of stratigraphic uplift of the basement in the rim ranged between 100 and 250 m.

In Fig. 2, the semi-annular area of the eroded breccia layer outlines the perimeter of the structure. The top of impact-deformed target rocks and ejecta is truncated by a discontinuity, which formed due to post-impact (Middle Ordovician) local marine shoreline erosion. Within the crater, as a result of post-sedimentary compaction, the top of the breccias is at depths of 295 to 100 m below present-day sea level (bsl), which is probably deeper than during the accumulation. Within the semi-annular zone of the missing allochthonous breccia, this discontinuity surface lies at variable depths between 150 and 30 m, relating to the local topography. Within the rim, the surface of the crystalline basement ranges from depths of 30 m to heights of 6 m above the sea level. Further outside the rim, the surface of the distal ejecta is 50 to 100 m bsl. In the further surroundings of the crater, the top of the pre-impact target is at depths of 60 m in the north to 100 m in the south due to the post-impact oblique regional sinking of the Baltic sedimentary basin. The ejecta layer that is preserved in the surroundings of the crater is thickest, up to 25 m, at distances of 3–6 km from the crater center. Erosion of the proximal part of the ejecta layer took place soon after the impact event because, during 5–10 Ma, the crater rim remained as an atoll-like feature, where it was subjected to erosion in the shallow sea. The crater depression represented a sedimentary trap with a higher accumulation rate, especially during the early post-impact times.

The crater was gradually buried under sediments over 5–10 Ma. During the Silurian and Devonian eras, the structure was probably buried under a 500 m-thick blanket of sediments. The Oslo rifting and tectonic-thermal event in western part of the East European Craton (including the Baltic Sea region) happened in the Late Carboniferous-Early Permian era, e.g., at about 300 Ma. Regional dolomitization and base metallic sulfide mineralization in Estonia is a manifestation of this activity (Puura et al. 1996). The post-

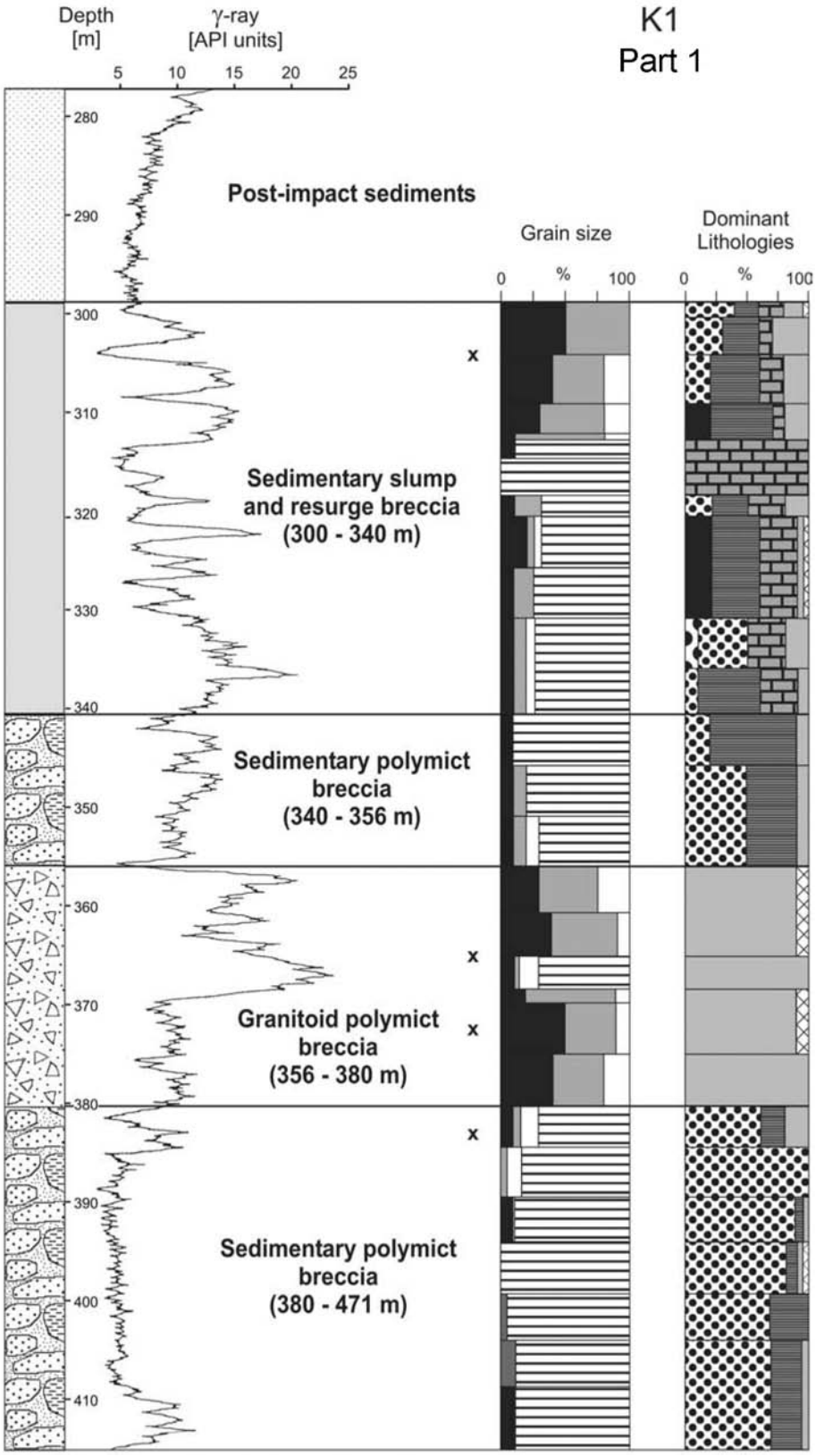

Fig. 4a. Lithological log of the drill core, grain size distribution, and lithological composition of allochthonous breccias from the crater interior in borehole K1 (part 1). Visual logs with γ-ray graphs are given in American Petroleum Institute (API) units (normalized for counts per second). The lithological composition is based on visual counting and the γ-ray log. "x" marks the positions of samples taken for geochemical analyses.

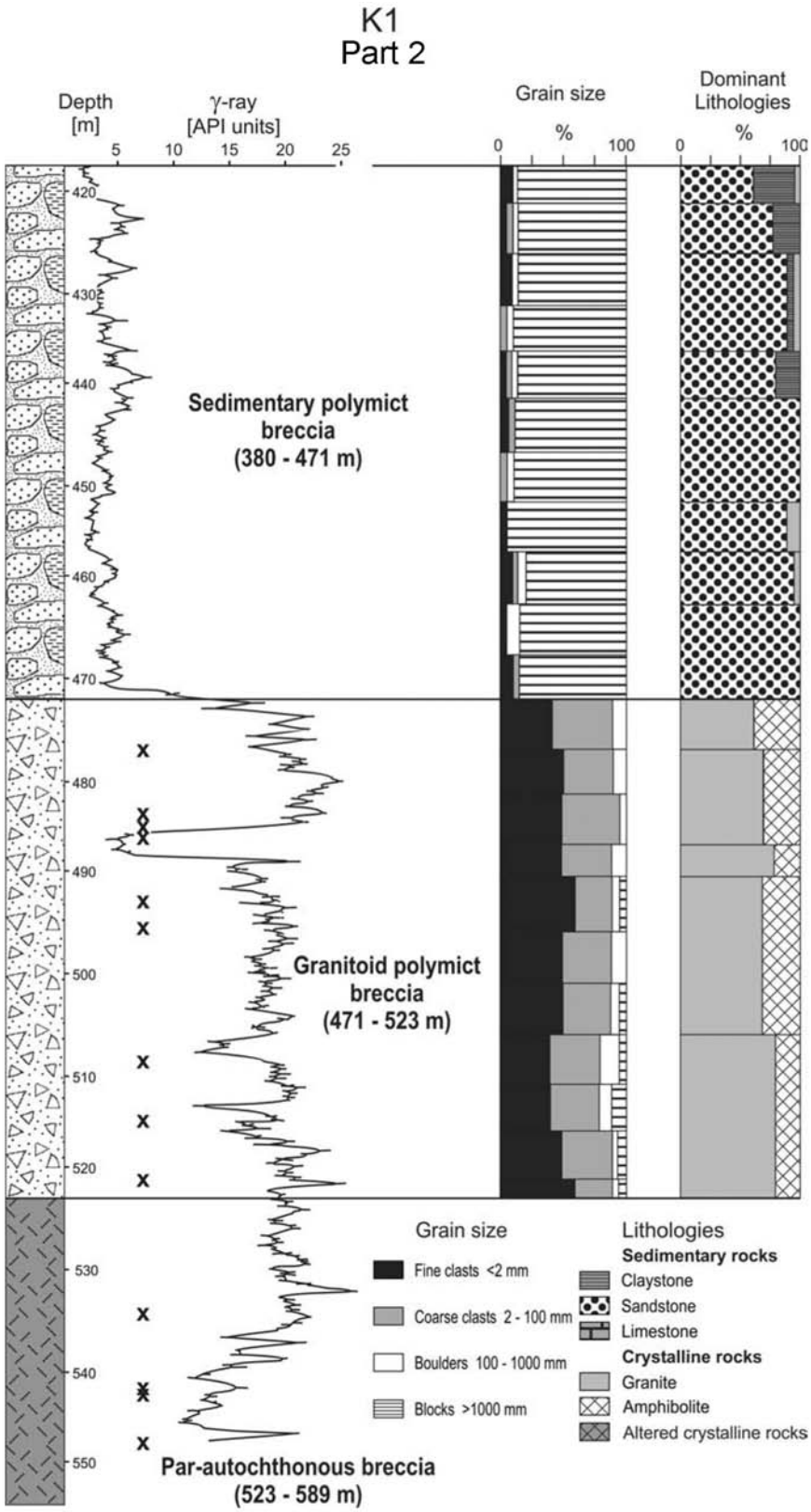

Fig. 4b. Lithological log of the drill core, grain size distribution, and lithological composition of allochthonous breccias from the crater interior in borehole K1 (part 2). Visual logs with γ-ray graphs are given in American Petroleum Institute (API) units (normalized for counts per second). The lithological composition is based on visual counting and the γ-ray log. "x" marks the positions of samples taken for geochemical analyses.

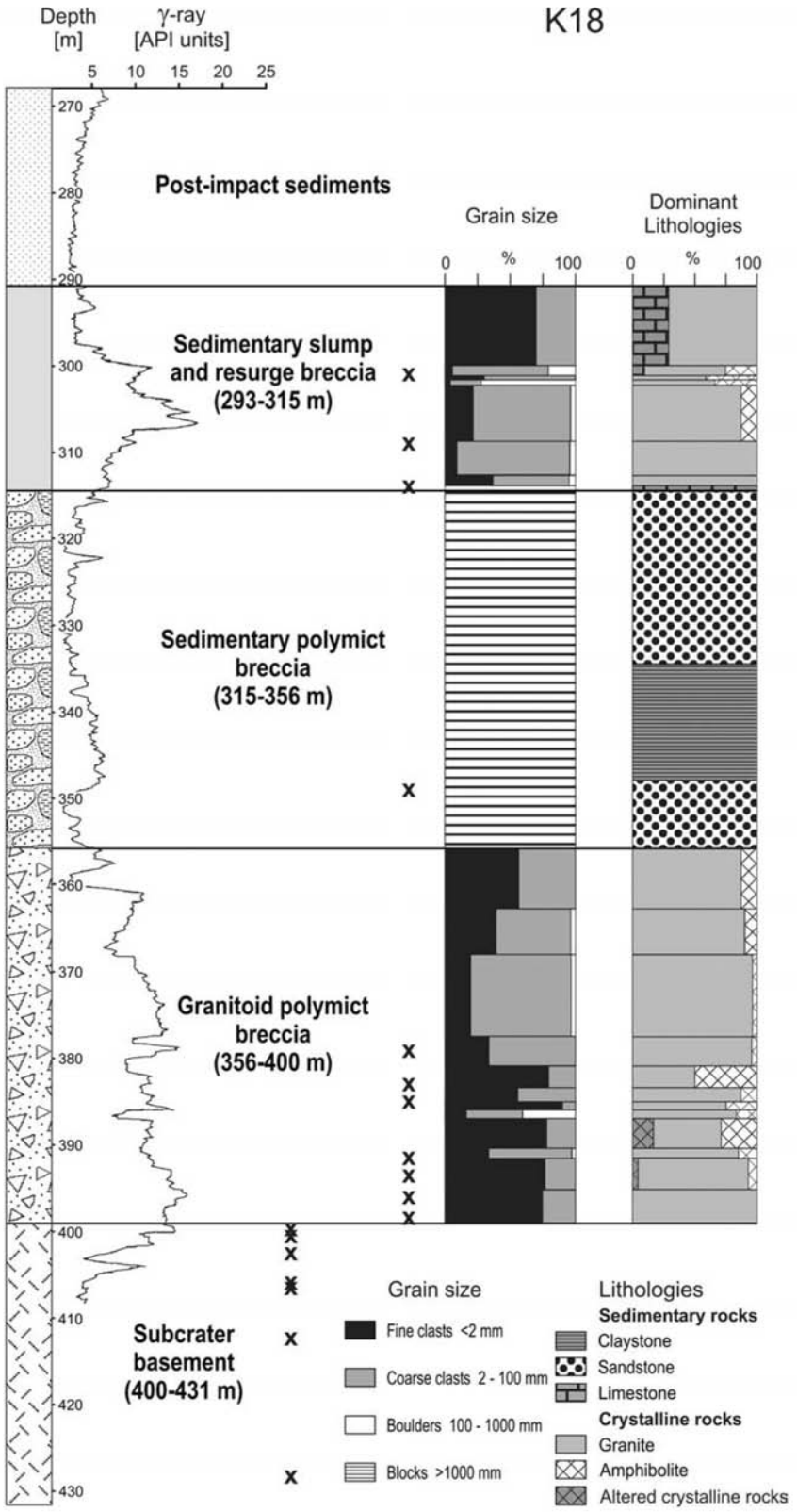

Fig. 4c. Lithological log of the drill core, grain size distribution, and lithological composition of allochthonous breccias from the crater interior in borehole K18. Visual logs with γ-ray graphs are given in American Petroleum Institute (API) units (normalized for counts per second). The lithological composition is based on visual counting and the γ-ray log. "x" marks the positions of samples taken for geochemical analyses.

impact lead and zinc sulphide and related carbonate mineralization in the Kärdla rim wall and covering sedimentary rocks belong to this event and, consequently, are not related to the impact-event. During the Mesozoic and Cenozoic eras, it was gradually unroofed. The Cenozoic erosion (see Puura and Flodén 1997) essentially uncovered the Kärdla impact site.

Settings of Studied Rock Units

Mixing of the debris produced from the almost 200 m-thick sedimentary layers and 300-m-thick portion of the crystalline basement appears to be incomplete. The approximately 50-m-thick allochthonous breccia unit that overlies the sub-crater basement is derived mainly from crystalline granitoids and amphibolites of the basement (core K1, 471–523 m; see Fig. 4b). This layer contains the most strongly shocked mineral fragments (shock pressures of 20–35 GPa). The other 30-m-thick layer of the same composition and with similarly shocked mineral clasts was penetrated at depths between 356 and 380 m, being separated from the lower layer by the mainly sedimentary rock-derived allochthonous, slumped breccia layer (380–471 m) without any admixture of shock metamorphic minerals. The second crystalline-derived breccia layer is covered with the uppermost, dominantly sedimentary-derived slumped, resurge and air-fall breccias (300–356 m) with occasional admixture of clasts of crystalline rocks and crystalline-derived breccias. We assume that the upper layer of crystalline-derived breccias with shocked minerals (356–380 m) is derived due to slumping of the uppermost parts of the rim wall, where the lower breccia unit is presently lacking, into the annular moat of the crater. The impact breccias of these two layers show the most intense evidence for the potassium enrichment and the sodium and calcium depletion. Inter-layers and patches of this breccia with signatures of K-metasomatism are met also within the sedimentary-derived layers of the slump breccia.

The sediment-derived breccia layers consist mainly of large blocks, cobbles, and pebbles of very soft rocks subjected to low shock pressure. The material probably slid back into the crater via gullies that existed in the crater rim. Observations on drill cores indicate that the sediment-derived allochthonous breccias lack any other major secondary mineralization.

The sub-crater basement has also been subjected to impact-induced fracturing and brecciation at low shock pressures reaching ~2 GPa in the par-autochthonous breccia unit in drill core K1. The K-enrichment and Na-Ca-depletion is gradually decreasing downward. However, the total volume of K-enriched rocks is much larger than the volume of rocks with obvious shock-metamorphic signatures.

In the geochemical study, we concentrate on: 1) impact-metamorphosed rocks of the allochthonous crystalline-derived breccia units; 2) rocks of the sub-crater basement as the main source for the breccias; and 3) the possible admixture of an extraterrestrial component.

SAMPLES AND ANALYTICAL TECHNIQUES

Optical Microscopy

Optical microscopy was performed on 175 thin sections at the Institute of Geology, University of Tartu and the Institute of Earth Sciences, Oulu University (see the Appendix for detailed descriptions). The orientations of planar deformation features (PDFs) in quartz grains were measured in 32 thin sections from drill cores K1 and K18 using standard universal stage (U-stage) techniques (see French 1998). Electron microscopic studies were performed using a JEOL 6300 scanning electron microscope (SEM) equipped with an Oxford ISIS energy dispersive spectrometer and a JEOL JSM-6300F field emission SEM at the Institute of Electron Optics, University of Oulu, Finland.

Electron Microprobe Analyses

Electron microprobe analyses (EPMA) of 20 thin sections were done with an automatized JEOL Superprobe 733 using 15 kV voltage, a 15 nA sample current, and a 5 or 10 μm electron beam diameter at the Institute of Electron Optics, Oulu University, Finland. The quantitative chemical compositions of silicate minerals were calculated using the ZAF correction program.

X-Ray Powder Diffractometry

The mineralogical composition of bulk-rock samples and K-feldspar fractions was determined using a Dron-3M diffractometer with Ni filtered CuKα-radiation at the Institute of Geology, University of Tartu, Estonia. Powdered rock samples were scanned at step widths of 0.02° 2θ in the range of 2 and 70° 2θ with time steps of 5–10 sec. Quantitative mineral composition of bulk-rock samples was found by full-profile Rietveld fitting, using the Siroquant 2.5™ (Taylor 1991) code. The XRD patterns of K-feldspar fractions were deconvoluted in the 20° to 40° 2θ region into elementary peaks using the Axes-19a code (Mändar et al. 1996). The measured diffraction peaks were fitted with symmetrical pseudo-Voigt function shape curve doublets. Relative abundances of the K-feldspar structural varieties (crosshatched twin structure microcline and orthoclase) were estimated from integral intensities of triclinic microcline (131) and ($1\bar{3}1$) and monoclinic orthoclase (131) peaks.

Geochemical Analyses

Geochemical analyses were performed on 90 samples from both drill cores K1 and K18 and target rock samples

from outside the crater rim (cores F361 and F364; see Koppelmaa et al. 1996).

Major, minor, and trace element abundances of 51 samples were determined using instrumental neutron activation analysis (INAA) and X-ray fluorescence spectrometry (XRF). Rock samples were crushed manually in plastic wrap, then mechanically in an alumina jaw crusher, and were powdered using an automatic agate mill. XRF analyses were performed at the University of the Witwatersrand, Johannesburg, South Africa, for the determination of major and some trace element abundances (Sr, Y, Zr, Nb, Ni, Cu, V, and Ba) following procedures described by Reimold et al. (1994). These authors also give information on the precision and accuracy of this method.

Another 15 samples were analyzed for major and trace element composition using XRD (Török and van Grieken 1992) in the central laboratory of the Federal Institute of Geosciences and Natural Resources (BGR) in Hannover (Germany). For quantitative analysis, a wavelength-dispersive X-ray spectrometer (WD-XRF) was used with a chromium tube (PW 1480) and a rhodium tube (PW 2400). For details of measurement procedures, precision, and accuracy, see Török et al. (1996).

In the laboratory of the Geological Survey of Estonia, 58 samples were crushed in a jaw crusher with carbon steel jaws and powdered in a ceramic disc-mill for wet chemical analyses of major elements. For details, see Kivisilla et al. (1999).

Aliquots of about 150 mg were analyzed at the University of Vienna, Austria, with INAA together with the well-characterized standard reference materials: the granites AC-E and USGS G-2 (Govindaraju 1989), the Allende meteorite standard reference powder (Jarosewich et al. 1987), and (for Au and Ir) the mineralized gabbro PGE standard WMG-1 (Canmet 1994). Koeberl (1993) and Koeberl et al. (1987) described the details of instrumentation, methodology, precision, and accuracy.

In addition, the iridium content of seven samples was determined with the γ, γ-coincidence spectrometry system at the Institute of Geochemistry (University of Vienna). For details on the measurement procedure and instrumentation, see Koeberl and Huber (2000).

RESULTS AND DISCUSSION

Impact Stratigraphy and Lithology

The sequence of crater-related lithologies consists of, from the bottom to the top: a) presumably intact crystalline rocks of the deep basement; b) autochthonous and par-autochthonous fractured and brecciated rocks beneath the crater floor (sub-crater basement) and in ring walls; c) allochthonous breccias within the crater (<250 m thick) and outside the wall (ejecta layer ~25 m thick); and d) post-impact (cover) deposits.

To compare the different impact stratigraphic units, we studied a variety of samples from core sections, especially in the main core K1 (originally labeled as F373) and K18, as shown in Figs. 4a–4c and described in the Appendix.

Unaffected basement rocks were drilled outside the crater (F361, F364). Autochthonous fractured and brecciated rocks continue below the bottom of 815.2 m in drill hole K1. As estimated from geophysical data and reconstruction of the transient cavity, these deformed rocks may extend to a depth of 1000 m (Plado et al. 1996). Their total thickness, consequently, may exceed 500 m. In the subcrater rocks, dikes of fine-grained breccia are common but decrease in number and size with depth (in K-1, to a depth of 800 m). In brecciated rocks, the same matrix fills interstitial spaces. The contact between the fractured and brecciated rocks is gradual. The thickness of the strongly brecciated zone at the crater floor in core K1 is estimated at ~30 m, in K18, at over 30 m, and in the Paluküla rim wall, at over 100 m. This layer is covered by par-autochthonous breccias forming the uppermost part of the sub-crater basement in core K1.

In the studied cores in the crater (K1, K18), up to five different impact-derived allochthonous crater-fill layers can be distinguished (Fig. 4). Cores K12, 412, and 383 (for locations, see Fig. 2) were investigated only macroscopically.

In the crater depression, horizontal allochthonous crater-fill layers conceal the central uplift. They perfectly leveled the crater floor before the post-impact sedimentation started. On the inner slopes of the crater, breccia layers thin out at depths that are not much higher than the central uplift (see Fig. 3). The youngest impact-related sediments (laminated carbonate-siliciclastic muds) cover a large area and were probably deposited from post-impact suspension-rich water. In gullies, this sediment also covers the lowest portions of the rim.

The regular concentric internal structure of the allochthonous impact breccias suggests that they formed early during the active modification stage. The lowermost unit of crystalline-derived breccias (K1, 523–471 m) is of almost par-autochthonous composition and probably formed along the contact of the impact plume and transient cavity floor. The second unit (K1, 471–380 m), composed of sedimentary-derived breccia, probably filled the moat around the rising central uplift during the early slumping process. The third layer of crystalline-derived breccias (K1, 380–356 m) is similar in texture and composition to the first unit and may have formed by slumping of parts of the first layer that were deposited at or near the crater rim. The crystalline-derived breccias of the first and third layers are dominantly monomict containing only small grains of sedimentary material. The fourth layer (K1, 356–300 m) is composed mainly of sedimentary rocks with a few clasts of crystalline rocks. In the upper part of this unit (~315 m), the abundance of crystalline clasts increases. In the northeast of the crater rim, at Paluküla High (core P11), matrix-rich impact breccia was found in pockets within the fractured crystalline rock.

In the first and third crystalline-derived breccia units, the matrix is also usually crystalline-derived. Crystalline-derived allochthonous breccia matrix is more or less strongly welded, suggesting hot deposition. Mixing of crystalline and sedimentary material in the plume is indicated by fine clastic sand to pelitic particles in the upper layers of the breccia matrix. Sedimentary-derived breccias of the third and fourth layers consist of large blocks and smaller fragments of sandstone, claystone, and limestone (Fig. 4). They are cement-poor and mainly of slump origin. Inter-clast cement is present as soft sedimentary rock powder with clasts of sedimentary origin. Larger fragments of crystalline material are found mainly as lumps of larger clasts already enveloped in fine impact-welded crystalline-type cement.

Slumping processes were essential during the formation of the within-crater stratigraphy. Thinning of the lower breccia layers toward the central uplift and all breccia layers toward the crystalline rim wall at Paluküla can be observed. Replacement, deformation, doubling, and even tripling of early breccia layers could have taken place.

Late resurge processes accumulated coarse-grained material, such as blocks, cobbles, pebbles, and gravel and were replaced by gradational sedimentation, first of gravel and sand and then of carbonate mud. Post-impact Late Ordovician carbonate sedimentation filled the crater depression, and later, Silurian sediments covered the impact site.

Spatial Distribution of Shock Metamorphic Features and Impact-Induced Alteration of Minerals

Shock metamorphic features were seen in quartz, microcline, and biotite. Due to impact-induced alteration, plagioclase and hornblende were replaced by submicroscopic orthoclase and chlorite aggregates (see Table 1). Distinct shock metamorphic features are found only in minerals of the allochthonous breccia. The volume of rocks subjected to chemical/mineralogical alteration is considerably larger, comprising also parautochthonous breccias and the fractured sub-crater basement.

Deformation of Quartz

Quartz with micro-scale fractures and voids is characteristic for a large volume of both allochthonous and autochthonous impact-affected rocks (Puura et al. 2000a). PDFs in quartz were found predominantly in crystalline rock clasts of the granitoid-dominated polymict breccia from cores K1 and K18 and in slump breccia from K1. In addition, weakly developed PDFs were found in quartz grains from proximal ejecta (cores K14, K15, K19 in Fig. 3), which are mainly composed of rounded quartz from Cambrian sand- and siltstone, with few mineral clasts derived from the crystalline basement. No PDFs were found in quartz from the autochthonous and par-autochthonous sub-crater basement, from crystalline rocks of the rim wall, or from the lower polymict breccia unit with sedimentary clasts and upper units with sedimentary and crystalline clasts. Diaplectic glass was not found.

The PDF orientation data obtained by U-stage studies of thin sections from the granitoid polymict breccia samples are given in Fig. 5. The number of PDF sets in quartz crystals from different units is typically one or two, with a maximum of three sets (Fig. 6). The abundance of PDFs decorated with fluid inclusions is low, amounting to only 1/3 of the undecorated PDF systems. The crystallographic orientation of PDF systems against quartz optical axis gives very broad maxima at $\{10\bar{1}3\}$ (ω) (Figs. 5a and 5b). The distribution patterns of the upper parts of K1 and K18 display a second maximum at an angle slightly lower than that of the $\{10\bar{1}2\}$ (π) orientation. This could be due to the binning (3° in Fig. 5a) or could indicate a problem with the precision of the

Table 1. Summary of the state of rock-forming minerals in different units (rim, K1, K18) of the Kärdla crater that were subjected to impact-induced alteration and replacement.[a]

Unit	Depth (m)	Microcline	Plagioclase	Hornblende	Biotite
Subcrater basement					
K1	620.0–815.2	Fresh	Or, relict or fresh Pl	Fresh, relict Hbl	Fresh, rare Chl
	589.0–620.0	Fresh	Or, relict Pl	Chl	Fresh, rare Chl
K18	400.0–431.4	–	Or, relict Pl	Chl	Fresh
Rim wall	–	Fresh	Or, fresh, relict or weathered Pl	Chl, relict Hbl	Fresh, Chl
Par-autochthonous basement					
K1	522.8–589.0	Fresh	Or, relict Pl	Chl	Fresh, rare Chl
Allochthonous crystalline-derived breccia					
K1	471.0–522.8	Fresh, Or	Or	Chl	Fresh, rusty patches
	356.0–380.0	Fresh, Or	Or	Chl	Fresh, partly Chl
K18	356.0–400.0	Fresh, Or	Or	Chl	Fresh, partly Chl
K1	300.0–340.0	Fresh, Or	Or	Chl	Fresh
K18	292.7–340.0	Fresh	Or	Chl	Fresh

[a]Or = orthoclase, Pl = plagioclase, Hbl = hornblende, Chl = chlorite.

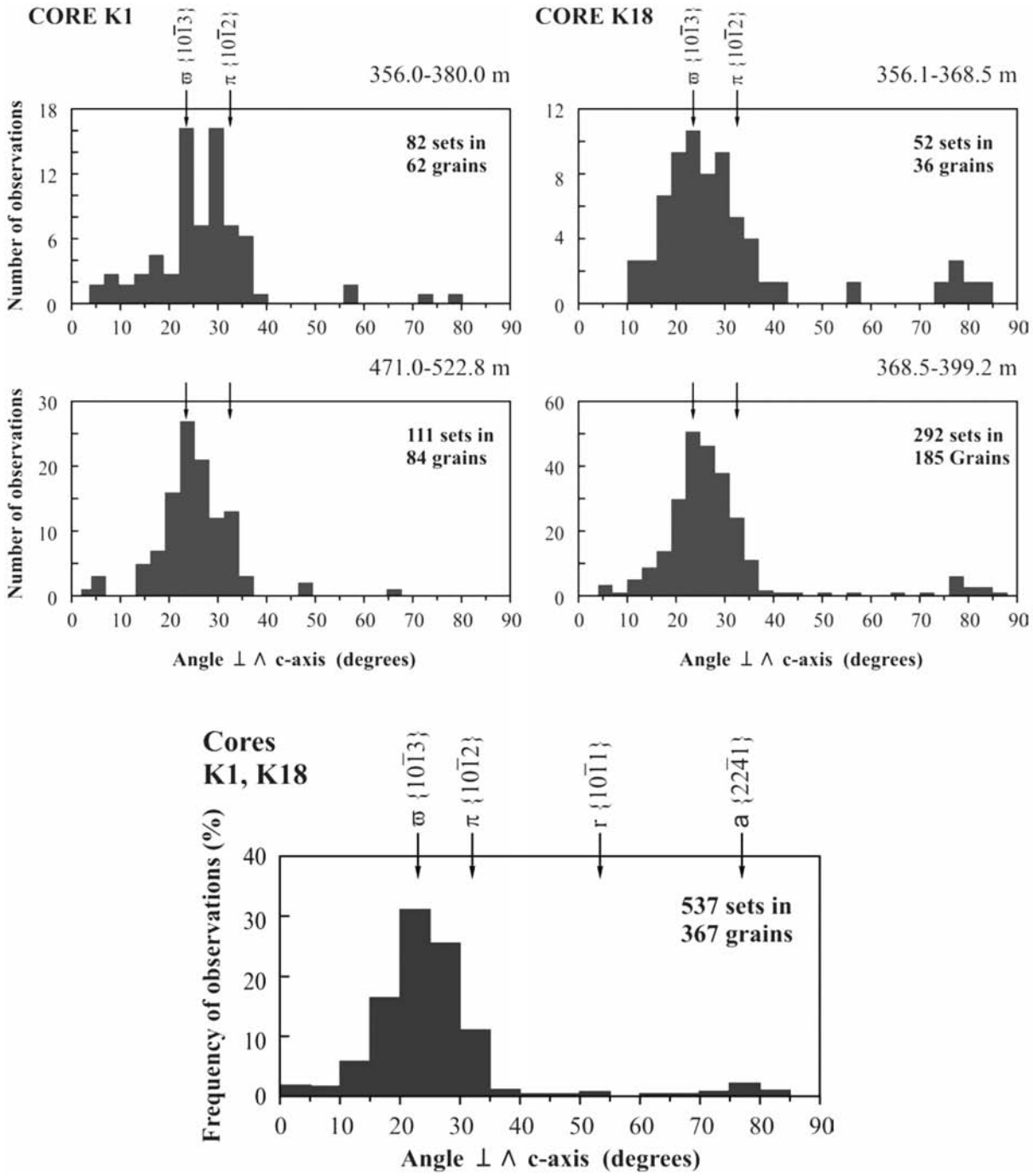

Fig. 5. Distribution of PDF orientations in quartz of granite-derived polymict breccia samples from cores K1 and K18. Top: histograms showing the number of PDF planes in 3° binning versus the angle between the c-axis and PDFs. Bottom: histogram combining all sets from the top with 5° binning.

measurements. This could also be the reason for the high percentage of unindexed planes (about 50%, by the method of Grieve et al. [1996]). In the lower parts of cores K1 and K18, the distribution of PDF orientations changes, indicating a dominance of ω orientations. The PDF orientations indicate a shock pressure in the range of ~10 to ≤35 GPa, with higher values characteristic for core K1and lower ones for K18.

Deformation and Alteration of Microcline

Primary microcline (Mc) with well-developed crosshatched twin structure has been mostly deformed and fractured by shock metamorphism. Inside the crater, microcline clasts with fractures and submicroscopic voids, rare deformation bands, and kink bands are observed. Microcline with planar fractures (PFs) and a ladder structure

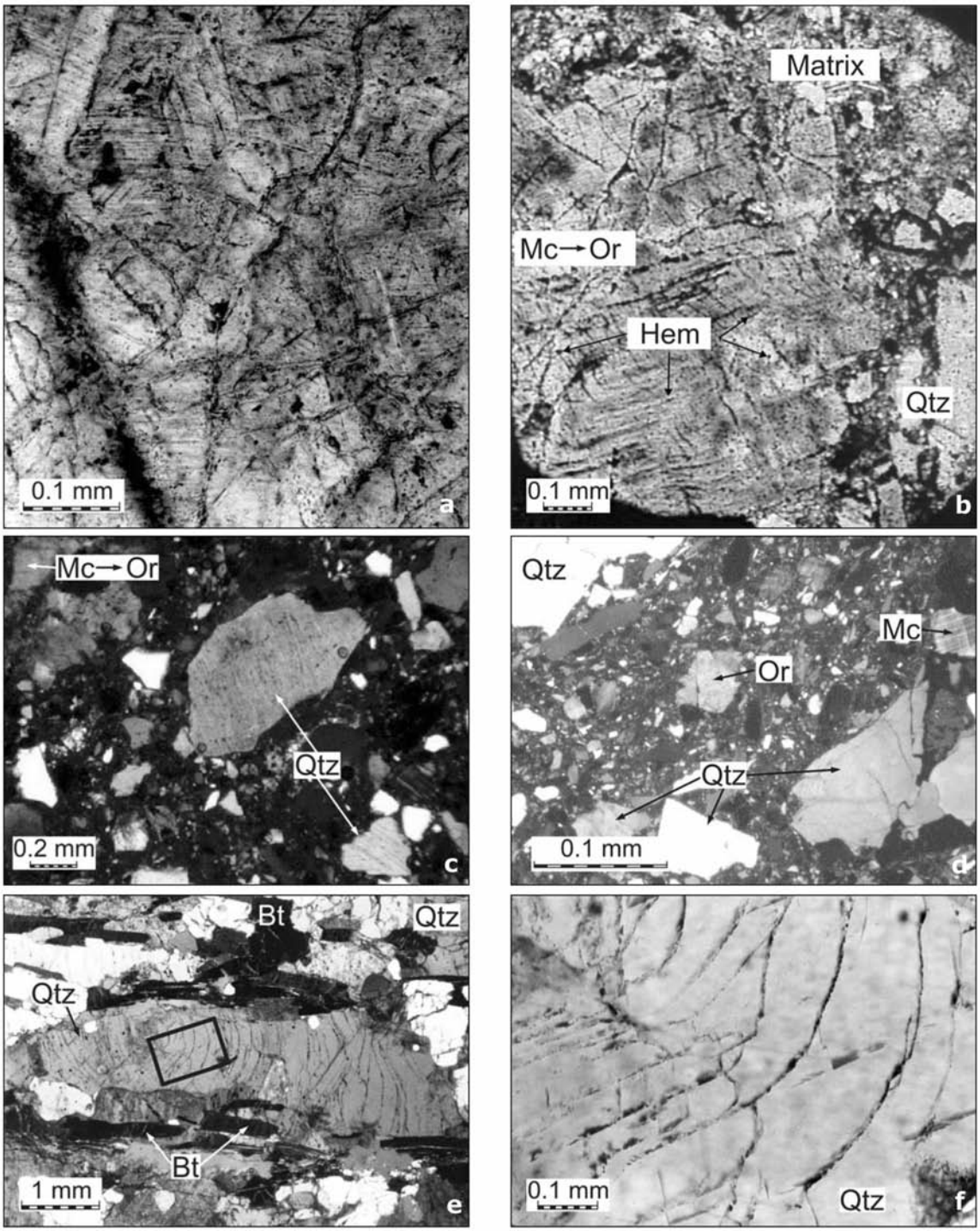

Fig. 6. Photomicrographs: a and b) allochthonous breccia on top of the central uplift, thin section K18-3830, (plane polarized light); a) a quartz (Qtz) clast with 3 sets of PDFs; b) microcline (Mc) replaced by secondary orthoclase (Or) that is pigmented by hematite (Hem). This large Or clast is kink-banded and crosscut by 3 systems of PDFs. The surrounding fine-grained matrix contains medium-sized quartz clasts; c) allochthonous breccia, thin section K18-3812, crossed polars. The breccia contains quartz clasts with one or two PDF systems and orthoclase replacing strongly deformed microcline, which has lost its primary twin structure; d) breccia dike, injected into the uppermost part of the sub-crater basement, thin section K1-6060, crossed polars. Quartz clasts are irregularly fractured and blocky. Microcline (Mc) either survived as a fragment with slightly deformed (kinked) twin structure or is replaced by secondary orthoclase without a crosshatched twin structure; e) sheared granite from near the base of the parautochthonous breccia layer; thin section of sample K1-5870 (plane polarized light). The large quartz fragment in the center displays crossing planar and sub-planar to conical fracture systems. The black rectangle corresponds to the close-up of (f); f) near the center of the cones, impact-related planar fractures divide the quartz grain into lamellae resembling tectonic Böhm lamellae.

occasionally occurs in rocks, which also contain PDF-bearing quartz (Fig. 6a). In places in the allochthonous breccia, the microcline twins are intensely deformed along multiple parallel fractures. In those samples, many microcline grains have partially or completely lost their optical evidences of polysynthetic twinning, which is in accordance with the results of XRD study. According to XRD data, the orthoclase/microcline (Or/Mc) ratio of K-Fsp megacrysts and clasts (Fig. 6b) varies from ~1 and less in the fractured sub-crater basement to 6–7 in the allochthonous breccia (Table 2; Fig. 7). Within the K-feldspar-yielding fine-grained allochthonous breccia matrix, and also in mm-size K-feldspar-yielding lithic clasts, the Or/Mc ratio increases up to 21. In crosshatched microcline from outside the crater, the Or/Mc ratio is around 0.1–0.2.

Large microcline clasts that derived from megacrysts of granitoids were found in the allochthonous breccia that includes abundant PDF-bearing quartz and were studied using backscattered electron images, EPMA, and XRD techniques. It was observed that, in the course of alteration, K-Fsp, indistinguishable from the surrounding K-Fsp, replaces perthitic lamellae. During this process, the Na and Ca contents of the primary perthitic microcline decreased (Puura et al. 2000b). In breccias devoid of shocked quartz and other shocked minerals, microcline clasts are mostly intact.

Alteration of Plagioclase and Hornblende

Primary plagioclase in biotite gneisses, granites, and amphibolites is in part replaced by submicroscopic orthoclase aggregates (Puura et al. 2000a). Partially altered plagioclase can contain relict plagioclase with polysynthetic twinning as well as cryptocrystalline orthoclase replacing the plagioclase (e.g., Fig. 8). The composition of primary and secondary feldspars is given in Table 3. Replacement by orthoclase is progressing along the plagioclase crystal rim and within crystal fractures and related micro-channels. The boundary between primary plagioclase and secondary orthoclase is sharp at the resolution of the microprobe (of about 5 μm). Voids less than 10 μm in diameter follow the impact-induced micro-fracture systems in replaced parts of the primary plagioclase crystals. This replacement is well-developed in both felsic and mafic rocks. In the allochthonous breccia containing quartz with PDF, secondary K-feldspar strongly dominates over primary plagioclase. In the sub-crater basement, partially altered plagioclase crystals and zoned rock clasts with both altered and unaltered plagioclases are found. Hornblende is the other mineral of mafic rocks sensitive to impact-induced alteration. In the allochthonous breccia, hornblende is totally replaced by an iron-rich chlorite and corrensite (Kirsimäe et al. 2002). In the sub-crater basement, some cm- to m-sized amphibolite bodies have a zoned structure. In their interior, almost fresh hornblende and plagioclase are preserved; along the perimeter and in fractures, hornblende is almost totally replaced by chlorite and plagioclase by orthoclase. In the sub-crater basement (cores K1 and K18), the content of altered hornblende decreases with depth.

Geochemistry

Major and Trace Elemental Composition

The results of the geochemical analysis are summarized in Table 4. The results of the individual analysis are available on request from the authors. The target rocks comprise mainly granites and amphibolites and accessory quartzites and limestone. The elemental abundances of the target rocks show considerable variations, but the different rock types still have distinct average compositions (Table 4).

Major element variations versus SiO_2-contents are shown in Harker diagrams (Fig. 9) for both target rocks (open symbols) and impact breccias (filled symbols). Amphibolites plot to the left (lower SiO_2-contents), limestone to the lower

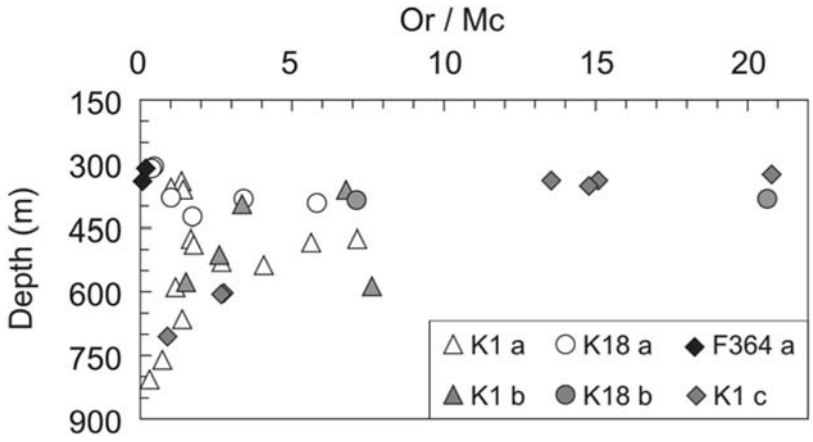

Fig. 7. Variation of orthoclase-to-microcline (Or-Mc) ratios with depth in rocks from cores K1 and K18 and, for comparison, from core F364 from outside the crater. a = K-Fsp clasts (megacrysts) in the breccia matrix, lithic clasts in the allochthonous impact breccia and in rocks of the sub-crater basement; b = K-Fsp-rich allochthonous breccia matrix; c = fine-grained K-Fsp in lithic clasts from the allochthonous breccia and the sub-crater basement.

Table 2. Orthoclase/microcline ratio (Or/Mc) determined by X-ray diffraction in various clasts, megacrysts, and bulk rock powder of impact breccias and sub-crater basement. The sub-divisions are according to Fig. 8. The numbers of the samples consist of the drill core designation (K1, K18, or F364) and the depth of sampling (in 0.1 m).

Sample	Or/Mc	Lithology
K-feldspar megacrysts and clasts		
Uppermost allochthonous breccia units		
K18-3066b	10.4	K-Fsp-Qtz aggregate clast in breccia matrix
K18-3112	0.34	K-Fsp-Qtz aggregate in granitoid clast
K1-3420	1.32	K-Fsp clast in breccia
Crystalline basement-derived allochtonous breccia units with PDFs in quartz		
K18-3803	0.97	K-Fsp clast in breccia matrix
K18-3830	3.36	K-Fsp clast in breccia matrix
K18-3930	5.78	K-Fsp clast in breccia matrix
K1-3570	0.97	K-Fsp clast in breccia matrix
K1-3610	1.37	K-Fsp-Qtz aggregate clast in breccia matrix
K1-4750a	7.10	K-Fsp inside of a 5 cm-size granite clast
K1-4750b	1.62	K-Fsp of fine chips from breccia matrix
K1-4836	5.59	K-Fsp megacryst in a migmatite clast
K1-4891	1.72	K-Fsp megacryst in granite block
Par-autochthonous breccia unit		
K1-5299	2.64	K-Fsp clast in breccia matrix
K1-5368	4.02	K-Fsp small clast (less than 1cm) in breccia matrix
Sub-crater basement units		
K18-4243	1.68	K-Fsp-Qtz aggregate in granite
K1-5895	1.12	K-Fsp-Qtz aggregate in granite
K1-6647	1.34	K-Fsp megacryst in granite
K1-7603	0.69	K-Fsp megacryst in granite
K1-8064	0.26	K-Fsp-Qtz aggregate in granite
Bulk rock powders from breccia matrix		
Crystalline basement-derived allochtonous breccia units with PDFs in quartz		
K18-3830	20.6	Breccia matrix
K18-3865	7.08	Breccia matrix
K1-3620	6.73	Breccia matrix
K1-3960	3.31	Breccia matrix
K1-5130	2.56	Breccia matrix
Par-autochthonous breccia unit		
K1-5770	1.47	Breccia matrix
K1-5870	7.58	Breccia matrix
Rock powders from basement, breccia matrix, and rock clasts		
Uppermost allochthonous breccia units		
K1-3255	20.8	Biotite gneiss clast
K1-3405b	13.5	Amphibolite clast
K1-3405d	15.0	Amphibolite clast
K1-3530	14.7	Breccia matrix
Sub-crater basement units		
K1-6030	2.71	Amphibolite
K1-6060	2.63	Granite
K1-7053	0.86	Granite
Basement rocks outside the crater rim		
F364-3425	0.06	Granite
F364-3110	0.19	Granite

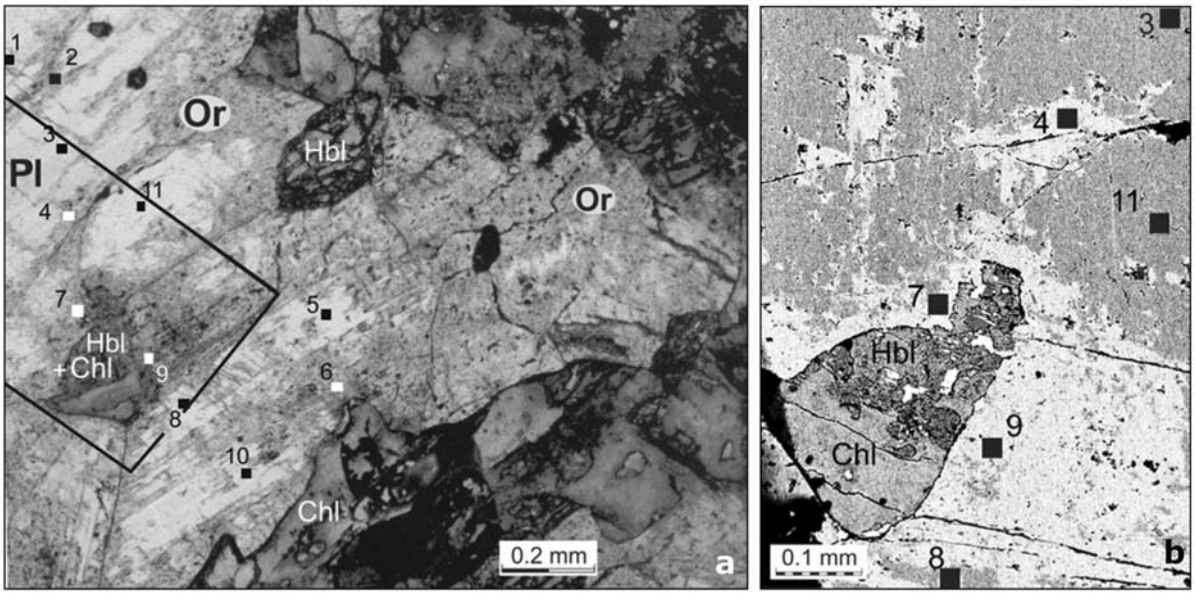

Fig. 8. Amphibolite K1-6030 from the sub-crater basement: a) photomicrograph, parallel polarizers. Electron microprobe analysis was used to determine the chemical composition of fresh and altered plagioclase (Pl). The numbers at the squares correspond to analyzes given in Table 3. The light colored area is a large crystal of plagioclase replaced by orthoclase (Or) at its margin and along micro-fractures. Plagioclase is surrounded by hornblende (Hbl), which is partly replaced by chlorite (Chl). The black frame corresponds to (b); b) BSE image. Plagioclase (grey) is replaced by orthoclase (white) at the lower right corner. In unaltered plagioclase, orthoclase is formed along fractures and porous regions. The inclusion of hornblende in altered pagioclase is partially replaced by chlorite.

Table 3. Electron microprobe (EMP) data for the chemical composition of a plagioclase grain partially replaced by orthoclase in amphibolite K1-6030 from the sub-crater basement (for analyzed spots, see Fig. 8).[a]

Sample	1	2	3	4	5	6	7	8	9	10	11
wt%	Pl	Or	Pl	Or	Pl	Or	Or	Pl	Or	Pl	Pl
SiO_2	56.9	61.8	55.7	61.4	57.2	60.2	62.5	57.2	61.7	57.8	57.4
TiO_2	–	–	0.04	–	0.01	0.02	–	0.02	–	0.04	0.06
Al_2O_3	23.6	16.7	24.4	17.0	23.6	16.6	17.3	23.5	16.8	23.6	23.5
MgO	–	–	–	0.01	–	–	0.06	0.01	–	–	–
FeO	0.06	–	0.03	0.05	0.15	0.23	0.30	0.13	0.15	0.09	0.06
MnO	–	–	0.01	0.08	0.04	0.11	–	–	0.01	0.02	–
CaO	6.68	–	7.45	–	6.51	0.23	–	6.47	0.02	6.87	6.90
Na_2O	7.96	0.07	7.32	0.04	8.00	0.12	0.09	8.14	0.05	7.99	8.17
K_2O	0.13	14.1	0.29	14.8	0.22	14.3	14.5	0.18	14.5	0.25	0.27
Total	95.33	92.67	95.24	93.38	95.73	91.81	94.75	95.65	93.23	96.66	96.36
Normative composition of the plagioclase grain.[b]											
Ab	67.8	0.7	63.0	0.4	68.1	1.3	0.9	68.8	0.5	66.9	67.2
An	31.5	0.0	35.4	0.0	30.6	1.3	0.0	30.2	0.1	31.8	31.4
Or	0.7	99.3	1.6	99.6	1.3	97.4	99.1	1.0	99.4	1.3	1.4

[a]Pl = plagioclase; Or = orthoclase.

[b]All data in %; Ab = Albite, An = Anorthite, Or = Orthoclase. Calibration of the EMP was done with the registered standard No. MAC 3056 of Agar Scientific Ltd., UK. The detection limits of the analyzed elements are about 0.01 wt%.

left, quartzites to the far right, and granites at about 70 wt% silica. While the contents of Fe_2O_3 and Al_2O_3 are linearly correlated in target rocks and breccias, K_2O is enriched, and Na_2O and CaO are generally depleted in the breccias compared to the target rocks. As mentioned, the K-enrichment results from the replacement of plagioclase by orthoclase and is prominent at many impact craters, e.g., at Boltysh (Gurov et al. 1986), Manson (Koeberl et al. 1996), Ames (Koeberl et al. 1997), Gardnos (French et al. 1997), or Ilyinets (Gurov et al. 1998). Generally, the target amphibolites have distinctly higher Sc, V, Cr, Co, and Ni but lower Hf and Th contents than the other basement rocks. The element ratios, such as K/U, Th/U, La/Th, and Hf/Ta, also indicate characteristic differences for each target lithology.

Table 4. Average compositions of target rocks and impact breccias from Kärdla crater.[a]

	Granite (25)		Quartzite (5)		Amphibolite (12)		Limestone (2)		Breccia matrix (13)		Breccia with granite clasts (17)		Breccia with amph. clasts (4)	
	Avg.	σ	Avg.	σ	Avg.	σ	Avg.	σ	Avg.	σ	Avg.	σ	Avg.	σ
SiO_2	72.4	3.0	83.0	2.7	47.8	3.2	49.2	12.1	67.9	6.2	77.3	8.4	51.5	1.1
TiO_2	0.40	0.17	0.21	0.07	0.97	0.36	0.17	0.02	0.71	0.47	0.37	0.22	0.84	0.23
Al_2O_3	12.3	1.6	7.22	1.27	15.2	1.3	0.79	0.01	12.2	1.3	10.0	3.4	13.3	1.7
Fe_2O_3	3.29	1.30	1.74	0.50	12.4	1.1	1.21	1.12	4.65	3.56	2.42	1.83	9.37	1.76
MnO	0.02	0.02	0.01	0.00	0.12	0.04	0.09	0.01	0.04	0.02	0.03	0.02	0.13	0.08
MgO	0.63	0.36	0.68	0.55	10.2	1.2	0.20	0.13	2.04	1.73	0.79	1.00	8.08	2.35
CaO	0.64	0.57	0.23	0.17	5.40	3.29	26.5	6.1	0.47	0.85	0.24	0.12	3.39	3.73
Na_2O	1.65	1.25	0.47	0.29	1.60	0.90	0.11	0.03	0.18	0.10	0.43	0.35	0.10	0.03
K_2O	6.81	1.19	5.10	1.06	2.59	1.48	0.39	0.26	8.54	1.46	7.02	2.19	5.75	0.55
P_2O_5	0.09	0.10	0.04	0.01	0.13	0.08	0.18	0.13	0.09	0.08	0.05	0.02	0.10	0.01
L.O.I.	1.02	0.63	0.84	0.64	3.38	2.47	21.3	5.1	3.07	2.36	0.87	0.41	7.43	2.30
Total	99.12		99.62		99.73		100.11		99.72		98.48		100.06	
Sc	5.23	2.74	2.09	1.38	39.7	5.4	1.37	0.63	12.8	4.9	4.61	3.65	37.1	17.9
V	17.7	22.0	21.8	10.4	291	72	14.3	9.5	84.5	44.2	34.3	28.0	205	49
Cr	3.7	2.7	19.1	15.8	263	130	10.4	0.5	46.9	20.8	16.6	16.3	130	36
Co	4.3	4.0	2.5	0.7	42.8	10.2	2.1	1.0	11.5	8.0	4.2	4.3	23.7	4.9
Ni	5.4	2.9	6.1	4.7	93.3	34.7	10.5	0.7	21.0	15.9	8.5	10.7	45.8	16.1
Cu	50.3	124	6.2	11.6	35.8	38.9	1.0	0.0	15.3	29.3	3.0	2.2	7.8	9.0
Zn	53.9	22.5	17.8	9.7	100	11.7	5.4	2.8	65.0	42.7	30.2	18.7	105	19.3
As	0.28	0.18	0.23	0.17	0.69	0.38	3.34	2.78	0.29	0.30	0.28	0.18	0.50	0.33
Rb	185	46.1	120	17.2	50	24	14.0	0.3	150	19	156	44	103	4 7
Sr	66.4	45.1	63.2	14.1	143	67.1	58.5	20.5	57.9	6.6	77.3	2.1	45.5	4.9
Y	47.1	20.2	13.4	5.9	28.6	17.6	8.0	1.4	42.3	45.0	28.2	20.7	38.5	5.8
Zr	382	192	109	26	83	61	135	66	226	45	218	127	131	61
Nb	15.0	4.4	7.2	2.9	11.8	6.8	7.0	0.0	15.5	5.3	12.2	5.2	20.0	8.3
Sb	3.43	6.05	2.23	4.90	0.31	0.21	0.21	0.11	5.01	6.96	5.77	6.49	0.26	0.24
Cs	1.34	0.93	1.10	0.81	0.67	0.42	0.36	0.17	2.38	1.13	1.82	1.13	1.42	1.12
Ba	735	514	584	55.6	148	32.9	90.7	35.6	742	278.1	869	288	365	229
La	131	73.5	31.8	23.5	13.0	10.4	10.0	4.1	65.4	39.6	40.9	13.7	23.9	18.5
Ce	226	127	50.3	24.0	28.4	19.7	17.6	7.2	105	45.2	78.6	30.8	49.7	34.9
Nd	84.3	58.2	19.4	8.3	14.2	7.8	9.1	4.8	39.7	19.2	31.8	11.9	23.7	15.7
Sm	13.8	9.8	3.38	1.54	3.36	1.91	1.94	1.15	7.62	4.12	5.85	2.93	5.29	3.25
Eu	1.16	0.27	0.57	0.03	1.13	0.44	0.39	0.18	1.28	0.56	1.03	0.66	0.92	0.18
Gd	11.4	6.6	3.19	1.56	4.20	2.23	2.00	1.07	7.17	5.13	5.02	2.49	6.51	3.24
Tb	1.58	0.96	0.45	0.15	0.81	0.43	0.35	0.18	1.22	1.04	0.76	0.45	1.25	0.56
Tm	0.61	0.29	0.24	0.10	0.55	0.38	0.16	0.02	0.62	0.52	0.29	0.26	0.71	0.18
Yb	3.83	1.91	1.48	0.72	3.87	2.85	1.00	0.02	4.02	3.23	1.81	1.65	4.89	1.02
Lu	0.50	0.24	0.20	0.11	0.59	0.42	0.15	0.01	0.55	0.39	0.25	0.24	0.72	0.13
Hf	9.44	3.57	3.13	0.92	1.97	1.25	4.12	2.26	4.38	1.68	3.39	1.75	3.63	1.61
Ta	1.27	1.00	0.77	1.00	0.74	0.63	0.20	0.01	1.56	0.81	1.45	1.17	1.30	0.62
Au (ppb)	7	3	5	3	5	2	1	1	5	2	5	1	6	1
Th	20.8	7.3	13.7	12.6	1.64	2.10	2.55	0.25	15.2	1.3	17.0	4.4	7.74	5.45
U	1.46	1.47	1.33	0.55	1.65	1.35	1.81	0.91	3.48	1.41	2.40	1.69	3.25	0.72
K/U	26520	14544	31918	16460	36144	47072	2370	2390	21760	8814	33527	16577	15084	2354
Th/U	9.15	4.08	10.3	8.97	1.62	2.01	1.57	0.64	4.90	1.61	11.05	7.77	2.60	2.08
La/Th	6.17	2.82	3.13	2.35	10.9	3.54	3.85	1.24	4.28	2.55	3.69	1.98	3.01	0.68
Zr/Hf	46.1	29.0	35.3	4.23	42.3	21.9	33.4	2.33	59.3	25.4	73.9	55.7	36.3	3.57
Hf/Ta	16.4	16.8	13.1	12.8	5.02	4.01	21.3	12.3	4.10	2.94	6.25	5.85	3.28	2.48
La_N/Yb_N	18.6	8.62	12.82	10.7	2.76	2.71	6.74	2.67	9.01	4.07	21.1	10.2	3.06	1.82
Eu/Eu*	0.35	0.15	0.62	0.24	1.03	0.45	0.62	0.08	0.57	0.13	0.56	0.07	0.55	0.17

[a]Major element data in wt%, trace elements in ppm, except as noted; all Fe as Fe_2O_3. The number of samples is given in parentheses. Individual analyses are available from V. Puura.

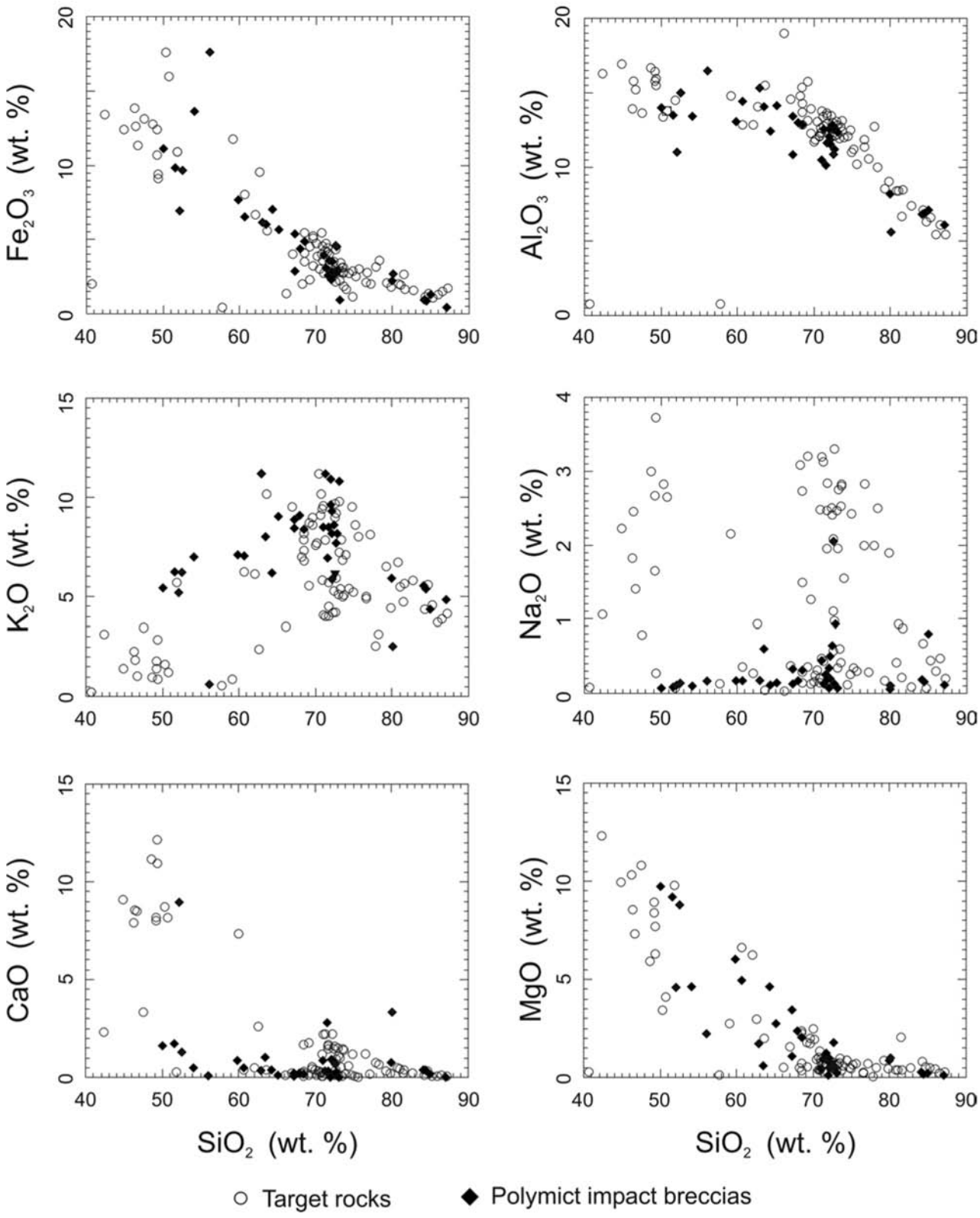

Fig. 9. Harker diagrams of target rocks and impact breccias from Kärdla crater. The contents of Fe_2O_3, Al_2O_3, and MgO are inversely correlated with that of SiO_2, with correlation coefficients of 0.87, 0.79, and 0.86, respectively. On the contrary, chemical alteration and K-metasomatism in the hydrothermal environment during and after the impact event led to highly variable patterns for CaO, Na_2O, and K_2O.

In Fig. 10, the variation of compatible and incompatible trace element compositions of allochthonous breccia samples and target rocks between elements is shown and indicates a minor admixture of amphibolitic component to mostly granitic breccias.

The average trace element composition of the impact breccias shows enrichments in the Ba, Cs, and U contents compared to the target rocks (Table 4). These enrichments are in good agreement with trace element distributions found, for example, at the Manson, Ames, or Gardnos craters (Koeberl et al. 1996, 1997; French et al. 1997). Impact-induced hydrothermal systems have been shown to be responsible for the mobilization of these elements in earlier impact crater studies (see, e.g., Reimold et al. 1994).

To further study the variations in the alkali contents, we used the ternary alteration diagrams by Nesbitt and Young (1989) shown in Fig. 11. In the A-CN-K (Al_2O_3-CaO + Na_2O-K_2O) diagram, unaffected amphibolites and mildly to strongly altered granites can be distinguished. In this diagram, K-metasomatism leads to a plot as shown in Fig. 11a, while weathering would lead to compositions in the direction of the dashed arrow (see Fedo et al. 1995). Two samples from the sedimentary allochthonous breccias plot outside of the range of these groups. One sample of sandstone seems to be unaffected, while a claystone-breccia is highly weathered, which is also visible in the A-CNK-FM diagram (Fig. 11b).

Chondrite-normalized rare earth element (REE) abundance patterns of three sample classes (breccias with granitic clasts, breccias with amphibolite clasts, and breccia matrix) are shown in Fig. 12. Breccia matrix includes samples without clasts larger than 2 mm. Averages and ranges in composition for the different rock types are presented in Table 4 and Fig. 12. Figure 12a shows the average composition of the three groups of breccia samples compared to the average compositions of the target rock types granite, quartzite, amphibolite, and limestone. Figure 12b illustrates the ranges in abundances. The breccias display large variations in REE abundances, reflecting the wide range of target rocks. Patterns for granites, quartzites, and limestones have steep slopes and negative europium anomalies. Amphibolites show an almost flat pattern with no distinct Eu-anomaly and slight enrichments in the heavy REEs (HREE). The three types of breccia samples have REE patterns similar to the granites. The HREE enrichment indicates a moderate admixture of amphibolites.

Mixing Calculations

According to major and trace element data (see Figs. 9, 10, and 12), most breccia samples result from the migmatized granitic basement with only minor contributions of amphibolite or limestone. For quantitative modeling, we used a harmonic least-squares mixing (HMX) program (Stöckelmann and Reimold 1989), which allows inclusion of measurement and averaging errors. Separate treatment of the mixing parameters (i.e., major and trace elements) and use of a large number of input components (target rocks and breccias) characterize this highly versatile program. Another useful feature is the so called Pivot component, which allows

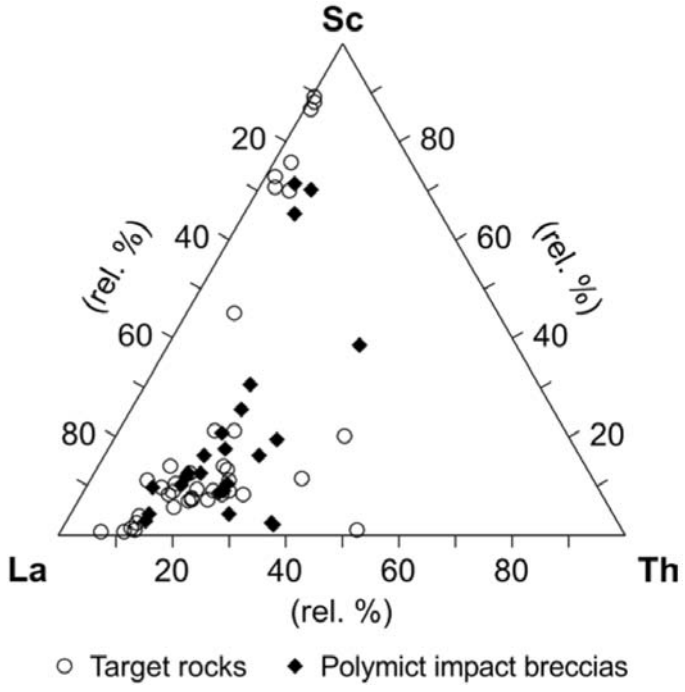

Fig. 10. Ternary diagram of La-Th-Sc showing the poor mixing of polymict allochthonous breccias. The two major types of target rocks, granites and amphibolites, plot close to the La (granites) and Sc (amphibolites) corner.

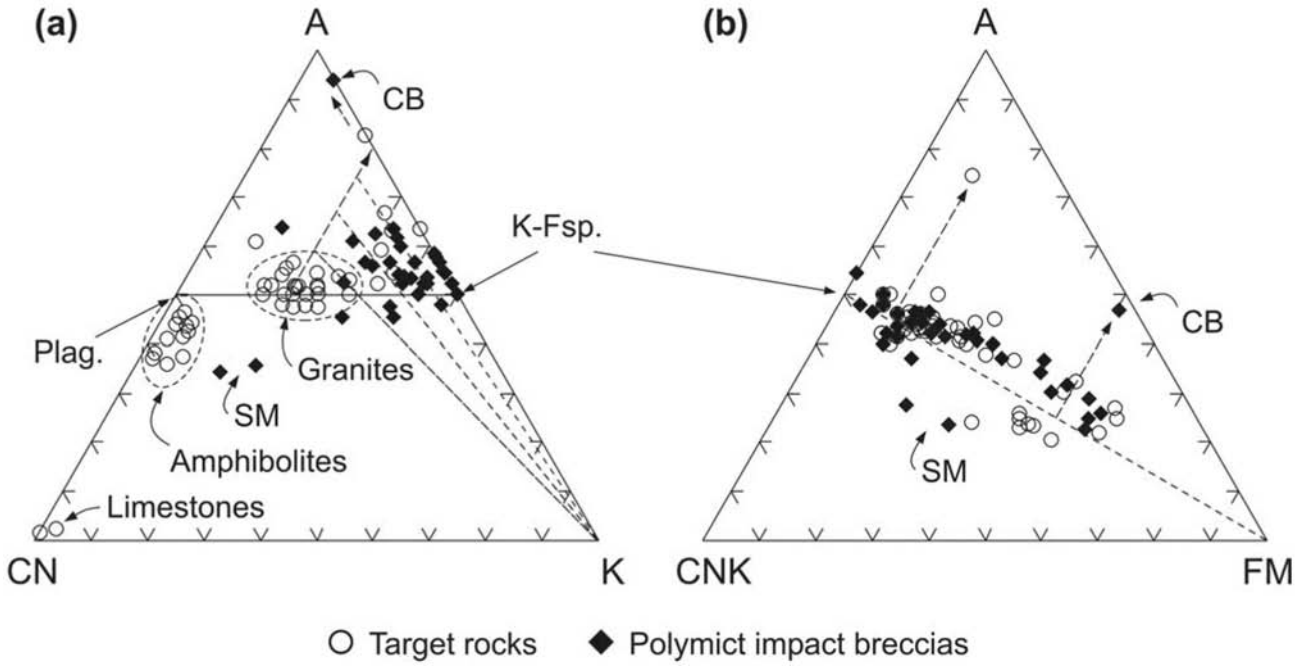

Fig. 11. Ternary diagrams for target rocks and impact breccias. A = Al_2O_3, C = CaO* (in silicate fraction only, corrected for phosphates and carbonates), N = Na_2O, K = K_2O, F = FeO_{total}, and M = MgO (in molar proportions). CIA = chemical index of alteration (for details, see Nesbitt and Young [1989]); CB = claystone breccia; SM = sandstone matrix. a) In the A-CN-K diagram, the general trends of alteration are drawn as dashed arrows. The breccias are mixtures of the amhibolites and granites of the basement, yet alteration causes a shift toward potassium. Plag. and K-Fsp. are idealized plagioclase and K-feldspar compositions, respectively (after Fedo et al. 1995); b) in the A-CNK-FM diagram, such high alteration values would shift the samples toward the A corner, but K-metasomatism neutralizes this effect. The stippled line represents the composition of unaltered granites. Only one breccia and one target sample show the "normal" weathering trend along the dashed arrows. In the A-CN-K diagram, these samples plot close to the Al_2O_3 corner.

one to force the presence of a certain component known to be present from petrographic studies in the mixture.

Calculations were performed on different breccia units from drill cores K1 and K18. These units comprise the allochthonous crystalline-derived polymict breccias at 471–523 m and 356–380 m depth in core K1 and 368.5–399.2 m and 356.1–368.5 m in core K18 (Figs. 4 and 5). For the target rocks (=input components), we used average compositions of granite, quartzite, amphibolite, and limestone (see Table 4). Average breccia compositions were modeled for three different types: breccia-bearing granite clasts, breccia with amphibolite clasts, and fine-grained breccia matrix (Table 4).

The parameters given in Table 5a were chosen to optimize the mixing conditions, as indicated by the lower discrepancy factors. These factors are a measure for the quality of the mixing calculation: zero means statistically optimized results, while results with factors of higher than five are of bad quality. The first run included all major elements except sodium and potassium, using all components with totals set to 100%. Run 2 was the same as run 1, but excluded limestone as a target component according to petrographic observations (Figs. 4a–4c). Runs 3 and 4 were designed similar to runs 1 and 2 but included Sc, Co, Y, Yb, and Th. These trace elements have the largest variations between different breccia types but the smallest variations within one breccia type. All mixing runs were first applied with and without fixed totals of 100 wt% to indicate any missing components. As differences between fixed and non-fixed totals were less than 1%, only results of runs with fixed totals are shown. The inclusion of trace elements led to a slight increase in the discrepancy factors. In spite of the high alteration of many samples, discrepancy factors are fairly low. For the granitic clast bearing breccia, and the average breccia matrix, the use of trace elements enlarge the amount of incorporated amphibolite, while, for the breccia with amphibolite clasts, a quartzite contribution could be excluded.

The calculations (Table 5a) yield the following results. The breccia matrix is mainly composed of granite, amphibolite, and subordinate quartzite. The breccia matrix can be reproduced by an admixture of ~80% granite and quartzite with a small contribution of amphibolite material. The amphibolite clast bearing breccia is composed of 70% amphibolites mixed with granite. The composition determined in run 4 is given in Table 5b. The average relative difference between observed and calculated abundances is 0.7% for all elements and <0.2% for the major elements. The highest differences between observed and calculated contents are found for the granite clast bearing breccia, and the amphibolite clast bearing breccia shows the lowest delta values. Generally,

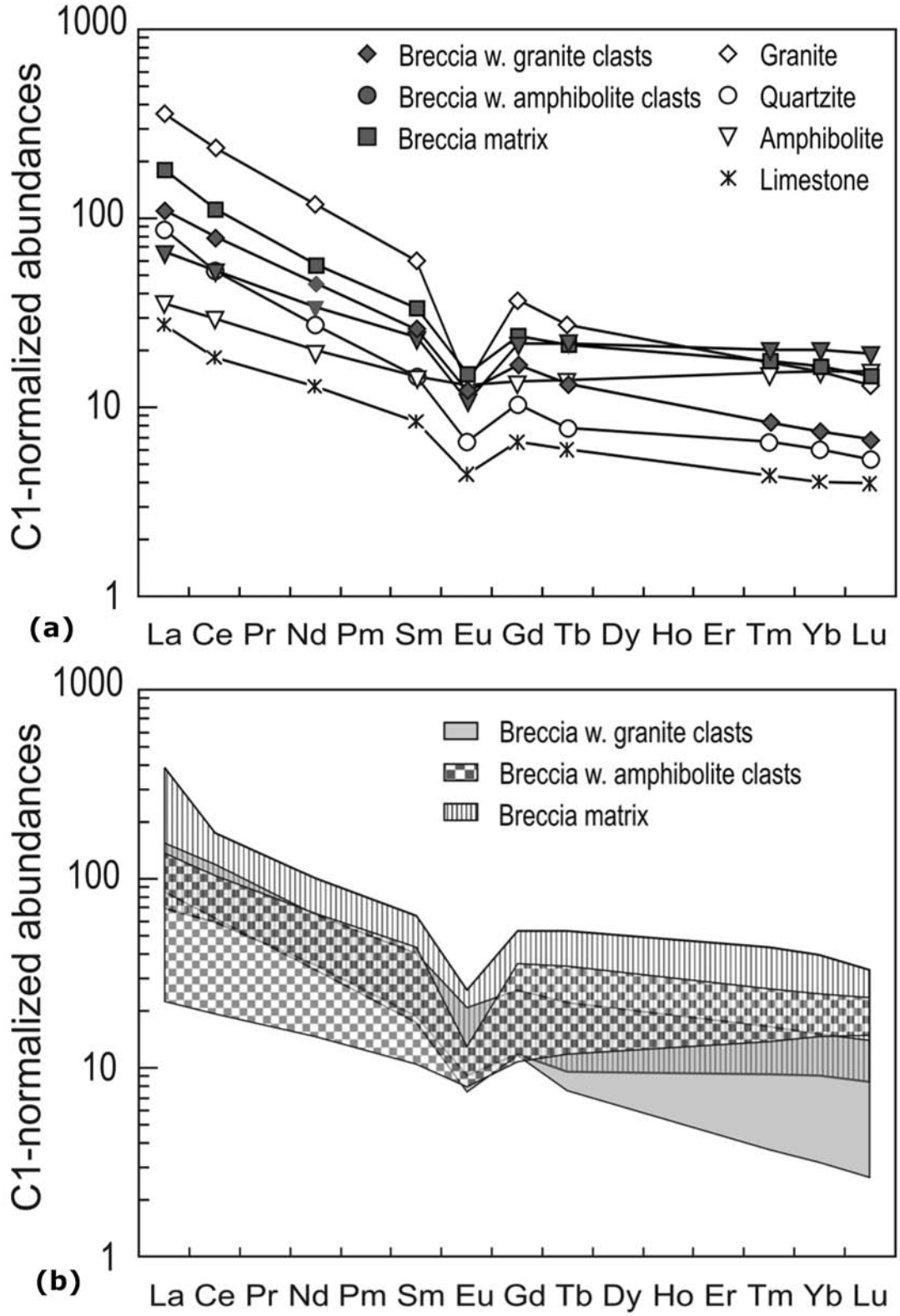

Fig. 12. Rare earth element plots of basement and brecciated samples normalized to C1-chondritic composition (Taylor and McLennan 1985) comparing (a) average breccias with average target rocks and (b) the ranges of different breccia types.

Table 5a. Parameters and results of mixing calculations to reproduce Kärdla impact breccias. The originally DOS-based HMX program (Stöckelmann and Reimold 1989) was adapted for Windows-based multi-sample input from an Excel spreadsheet (Huber 2003) to enable extensive mixing calculations for a large number of breccia samples.[a]

		Mixing components				
Mix	Run	Granite	Quartzite	Amphibolite	Limestone	Discrep. factor
Breccia matrix	1	86.6 ± 2.0	<1	11.1 ± 1.7	<0.7	2.7
	2	86.6 ± 2.1	<0.9	11.2 ± 1.8	–	0.9
	3	74.0 ± 2.6	6.9 ± 2.0	17.5 ± 1.2	<0.01	3.8
	4	73.8 ± 3.0	8.4 ± 2.3	17.9 ± 1.4	–	1.5
Granite clast bearing breccia	1	68.4 ± 5.7	31.6 ± 5.5	<0.7	<0.8	3.3
	2	68.4 ± 5.8	31.6 ± 5.7	<0.7	–	1.1
	3	57.4 ± 4.1	41.9 ± 4.0	0.8 ± 0.3	<0.01	5.1
	4	57.4 ± 4.5	41.9 ± 4.4	0.8 ± 0.2	–	1.8
Amphibolite clast bearing breccia	1	8.5 ± 3.4	11.4 ± 2.3	75.1 ± 0.9	<1.3	0.9
	2	8.5 ± 3.4	11.4 ± 1.6	75.1 ± 1.4	–	0.2
	3	26.4 ± 1.4	<0.01	68.5 ± 1.4	<0.01	5.3
	4	26.4 ± 1.5	<0.01	68.5 ± 1.5	–	1.2

[a]Runs: (1) total to 100%, all comp., all major elements without Na_2O, K_2O, LOI; (2) 1 without limestone; (3) 1 + trace elements (Sc, Co, Y, Yb, Th); and (4) 3 without limestone.

Table 5b. Comparison of calculated and observed composition for the three breccia sample types, based on run 4 of the mixing calculations.[a]

	Breccia matrix		Breccia with granite clasts		Breccia with amphibolite clasts	
	Calc.	$\Delta_{(Obs.-Calc.)}$	Calc.	$\Delta_{(Obs.-Calc.)}$	Calc.	$\Delta_{(Obs.-Calc.)}$
SiO_2	68.74	–0.82	76.62	–0.05	51.58	–0.04
TiO_2	0.50	0.21	0.33	0.05	0.81	0.03
Al_2O_3	12.31	–0.08	10.18	–0.08	13.56	–0.23
Fe_2O_3	4.78	–0.13	2.71	0.01	9.37	0.00
MnO	0.04	–0.00	0.02	0.01	0.09	0.03
MgO	2.33	–0.28	0.73	0.04	7.22	0.85
CaO	1.04	–0.57	0.34	–0.05	3.74	–0.35
Sc	11.4	1.3	4.32	0.63	28.9	8.1
Co	11.1	0.4	4.08	1.37	25.8	–2.2
Y	41.1	1.1	31.7	–3.5	37.4	1.1
Yb	3.71	0.31	2.51	–0.71	4.64	0.25
Th	15.2	–0.1	17.5	–0.1	6.79	0.96

[a]Data given in wt% (major elements) and ppm (trace elements).

SiO_2, Al_2O_3, FeO, Th, and Y show the smallest differences, while the values for MnO, CaO, and Sc differ highly.

Extraterrestrial Component

For the detection of an extraterrestrial component in impact breccias, contents of the siderophile element (e.g., Co, Ni, Cr, and Ir) can be used, which are highly enriched in chondritic and iron meteorites but have very low abundances in the upper continental crust. Due to the possible enrichment of these elements in amphibolites, the terrestrial input (indigenous component from the target rocks) has to be determined first. This was done on the basis of the HMX mixing results. The patterns of C1-normalized ranges for the siderophile transition metals (Fig. 13) show no or only minor enrichments indicative of an extraterrestrial component. In addition, the averages corrected for the indigenous components are shown. All averages plot below the normalized average upper continental crust (UCC) abundances (Taylor and McLennan 1985). Therefore, on the basis of this pattern, no accurate information on the amount of any extraterrestrial material can be given.

Iridium, on the other hand, is an element with abundances that can be measured with specific techniques (chemical separation or γ, γ-coincidence spectrometry) in the range characteristic of upper crustal values (about 20 ppt; after Taylor and McLennan 1985). The distribution of Ir within the seven samples analyzed by γ, γ-coincidence spectrometry points to only minor enrichment. Sample K18-3791, a granite clast bearing breccia, has a content of 128 ppt Ir that, compared to a background between 28 and 62 ppt Ir, may indicate a small extraterrestrial contribution. This sample was corrected for the indigenous component, and the pattern is shown in Fig. 13b. Although iridium and gold contents are slightly above average UCC abundances, the

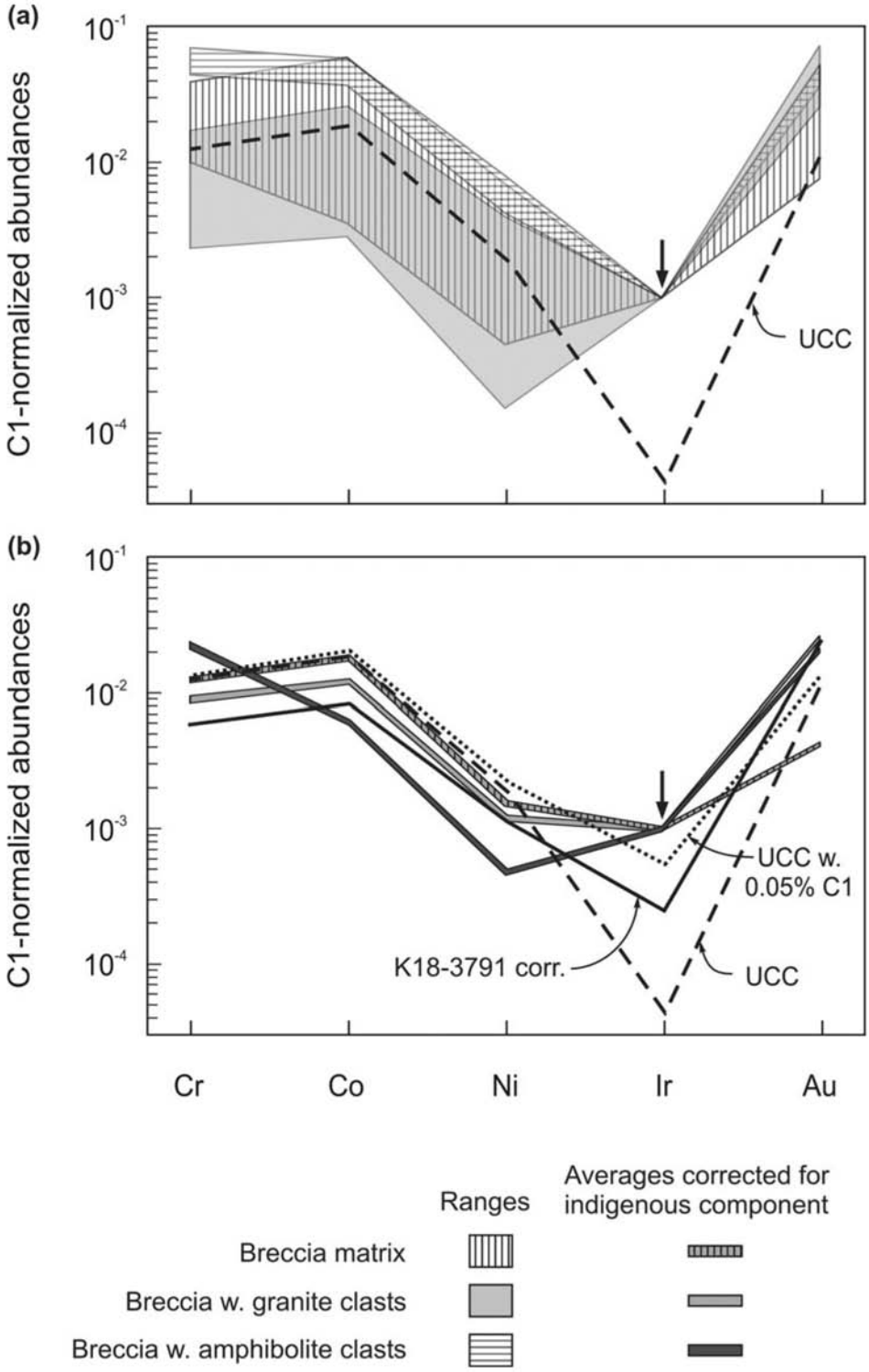

Fig. 13. C1-chondrite normalized siderophile element patterns of different breccia types. In (a), the ranges for the different breccia types are shown, while in (b), averages corrected for the indigenous component are presented. For comparison, the abundances of the upper continental crust (UCC) are shown as a dashed line. The iridium contents are below the detection limit of INAA at 0.5 ppb (black arrow). All average siderophile element contents in the breccias corrected for the indigenous component are below the average upper continental crust abundances. Sample K18-3791, showing elevated iridium abundances of 128 ppt, was plotted after correction for an indigenous contribution, leading to a pattern below the 0.05% mixing line for CI-chondritic material in UCC (dotted line; data from Taylor and McLennan [1985]).

pattern suggests a maximum incorporation of less than 0.05% of a C1-chondrite. This trend is in good agreement with recently presented mixing-parameters of projectile quantities for impacts on wet targets (Ryder 2001). A previously suggested iron meteorite as projectile for the Kärdla crater (Suuroja et al. 2002a) is rather unlikely based on the distribution patterns given in Fig. 13. For an iron projectile, variations of the Ni, Co, and Ir contents of at least three orders of magnitude would be necessary. The observed patterns are in better agreement with a very minor chondritic addition, but no clear assignment is possible due to the low abundances observed; for a confirmation of an extraterrestrial component, abundances and inter-elemental ratios of all platinum group elements (see McDonald et al. 2001) or isotopic studies would be necessary.

K-Enrichment and Na-Ca-Depletion of Minerals and Rocks

The Na-Ca-depletion and K-enrichment developed in strongly crushed and porous allochthonous and par-allochthonous crystalline-derived breccias and, to a lesser degree, in fractured sub-crater basement rocks. The alteration caused the replacement of plagioclase and minor microcline by orthoclase and of hornblende by chlorite-corrensite. In addition, some biotite was altered. These processes yielded a Na-Ca-depletion and enrichment with K. Besides the extensive formation of orthoclase pseudomorphs, hydrothermal chlorite and corrensite and carbonates (Kirsimäe et al. 2002) appear as fracture and vug fillings. In some places, the latter are accompanied by minor veinlets of K-feldspar, yet formation of the orthoclase pseudomorphs predates the vein- and vug-filling minerals.

In impactites, the formation of K-feldspar is usually explained by K-release during post-impact hydrothermal alteration of impact melt rocks (e.g., Grieve 1994; McCarville and Crossey 1996; Gurov et al. 1998; Masaitis et al. 1999; Naumov 2002; Vishnevsky and Montanari 1999). In the Kärdla structure, however, melt rocks and even suevites were not found so far. Our preliminary results indicate a paragenetic succession of mineral associations, starting with the wide-spread formation of orthoclase pseudomorphs after plagioclase from hot, possibly vapor-dominated fluids to subdued late microcrystalline K-feldspar, dolomite, and calcite, which crystallized from water-dominated fluid systems at approximately ambient conditions. Kirsimäe et al. (2002) give homogenization temperatures of 150–300 °C for fluid inclusions in quartz and 100–200 °C for the formation of corrensite-chlorite mineral pairs, corresponding to conditions during the hydrothermal stage.

CONCLUSIONS

The Kärdla crater was formed in a layered sedimentary and crystalline target in a shallow epicontinental sea. The crater-fill consists of sedimentary- and crystalline-derived allochthonous breccias, with their upper parts in secondary, slump, and resurge position. Only the crystalline-derived polymict allochthonous breccias contain intensely shock-metamorphosed minerals, including quartz containing PDFs indicating shock pressures of about 10–35 GPa. The allochthonous sedimentary-derived breccias, par-autochthonous crystalline-derived breccias, and sub-crater basement rocks lack quartz with PDFs. In the par-autochthonous crystalline-derived breccias and the uppermost part of the sub-crater basement, the presence of kinked biotite suggests shock pressures between ~2 and 6–10 GPa. Crystalline rocks are the major precursor rocks for the polymict breccias. Slight Ir enrichments indicate the incorporation of extraterrestrial material in very minor amounts, but an iron meteorite is unlikely as a projectile according to the inter-elemental ratios of siderophile elements. The K-enrichment and Na-Ca-depletion is ubiquitous at Kärdla in the crystalline-derived allochthonous and par-autochthonous breccias. In the sub-crater basement, it gradually decreases with increasing depth.

Acknowledgments–This work was supported by the Ministry of Education of Estonia (Project 0551) and Estonian Science Foundation (Grants 4417 an 5817 to V. Puura) and the Austrian "Fonds zur Förderung der wissenschaftlichen Forschung," project START Y58-GEO (to C. Koeberl). The authors are very grateful to O. Taikina-Aho and J. Paaso, operators at the Institute of Electron Optics, Oulu University, for SEM and EMPA analyses. We are grateful to the reviewers Erik Sturkell and Ray Anderson and to associate editor Alex Deutsch, for detailed and critical comments and helpful advice for improving the manuscript.

Editorial Handling—Dr. Alex Deutsch

REFERENCES

Abels A., Plado J., Pesonen L. J., and Lehtinen M. 2002. The impact cratering record of Fennoscandia: A close look at the database. In *Impacts in Precambrian shields,* edited by Plado J. and Pesonen L. J. Berlin: Springer Verlag. pp. 1–58.

CANMET 1994. Catalogue of certified reference materials. Canadian Certified Reference Materials project 94-1E. 82 p.

Fedo C. M., Nesbitt H. W., and Young G. M. 1995. Unraveling the effects of potassium metasomatism in sedimentary rocks and paleosols, with implications for paleoweathering conditions and provenance. *Geology* 23:921–924.

French B. M. 1998. *Traces of catastrophe: A handbook of shock-metamorphic effects in terrestrial meteorite impact structures.* LPI Contribution No. 954. Houston: Lunar and Planetary Institute. 120 p.

French B. M, Koeberl C., Gilmour I., and Shirey S. B. 1997. The Gardnos impact structure, Norway: Petrology and geochemistry of target rocks and impactites. *Geochimica et Cosmochimica Acta* 61:873–904.

Govindaraju K. 1989. 1989 compilation of working values and sample description for 272 geostandards. *Geostandards Newsletters* 13:1–113.

Grieve R. A. F. 1994. An impact model of the Sudbury structure. In

Proceedings of the Sudbury-Noril'sk symposium, edited by Lightfoot P. C. and Naldrett A. J. Special Vol. 5. Toronto: Ontario Geological Survey. pp. 119–132.

Grieve R. F., Langenhorst F., and Stöffler D. 1996. Shock metamorphism of quartz in nature and experiment: II. Significance in geoscience. *Meteoritics & Planetary Science* 31: 6–35.

Gurov E. P., Gurova E. P., and Kolesov G. M. 1986. Impactite composition of the Boltysh astrobleme. *Meteoritika* 45:150–155. In Russian.

Gurov E. P., Koeberl C., and Reimold W. U. 1998. Petrography and geochemistry of target rocks and impactites from the Iljinets Crater, Ukraine. *Meteoritics & Planetary Science* 33:1317–1333.

Huber H. 2003. Application of γ, γ-coincidence spectrometry for the determination of iridium in impact-related glasses, tektites, and breccias. Ph.D. thesis, Institute of Geochemistry, University Vienna, Austria.

IUGS 2000. *International stratigraphic chart, 2nd edition.* Paris: UNESCO Division of Earth Science.

Jarosewich E., Clarke R. S., Jr., and Barrows J. N., editors. 1987. The Allende meteorite reference sample. *Smithsonian Contributions to Earth Science* 27:1–49.

Kirsimäe K., Suuroja S., Kirs J., Kärki A., Polikarpus M., Puura V., and Suuroja K. 2002. Hornblende alteration and fluid inclusions in Kärdla impact crater, Estonia: Evidence for impact-induced hydrothermal activity. *Meteoritics & Planetary Science* 37:449–457.

Kivisilla J., Niin M., and Koppelmaa H. 1999. *Catalogue of chemical analyses of major elements in the rocks of the crystalline basement of Estonia.* Tallinn: Geological Survey of Estonia. 94 p.

Koeberl C. 1993. Instrumental neutron activation analysis of geochemical and cosmochemical samples: A fast and reliable method for small sample analysis. *Journal of Radioanalytical and Nuclear Chemistry* 168:47–60.

Koeberl C. and Huber H. 2000. Multiparameter γ, γ-coincidence spectrometry for the determination of iridium in geological material. *Journal of Radioanalytical and Nuclear Chemistry* 244: 655–660.

Koeberl C., Kluger F., and Kiesl W. 1987. Rare earth element determination at ultratrace abundance levels in geologic materials. *Journal of Radioanalytical and Nuclear Chemistry* 112:481–487.

Koeberl C., Reimold W. U., Kracher A., Träxler B., Vormaier A., and Körner W. 1996. Mineralogical, petrological, and geochemical studies of drill cores from the Manson impact structure, Iowa. In *The Manson impact structure: Anatomy of an impact crater,* edited by Koeberl C. and Anderson R. R. Special Paper 302. Boulder: Geological Society of America. pp. 145–219.

Koeberl C., Reimold W. U., Brandt D., Dallmeyer R. D., and Powell R. A. 1997. Target rocks and breccias from the Ames impact structure, Oklahoma: Petrology, mineralogy, geochemistry, and age. In *Ames structure in northwest Oklahoma and similar features: Origin and petroleum production,* edited by Johnson K. S. and Campbell J. A. Circular 100. Norman: Oklahoma Geological Survey. pp. 169–198.

Koppelmaa H., Niin M., and Kivisilla J. 1996. About the petrography and mineralogy of the crystalline basement rocks of the Kärdla crater area, Hiiumaa Island, Estonia. *Bulletin of the Geological Survey Estonia* 6:4–24.

Mändar H., Vajakas T., Felsche J., and Dinnebier R. E. 1996. AXES 1.4: A program for the preparation of parameter input files for FULLPROF. *Journal of Applied Crystallography* 29: 304.

Masaitis V. L., Naumov M. V., and Mashchak M. S. 1999. Anatomy of the Popigai impact crater, Russia. In *Large meteorite impacts and planetary evolution II,* edited by Dessler B. O. and Sharpton V. L. Special Paper 339. Boulder: Geological Society of America. pp. 1–17.

Masaitis V. L., Pevzner L. A., Deutsch A., and Ivanov B. A., editors. 2004. *Deep drilling in the Puchezh-Katunki impact structure, Russia.* Heidelberg: Springer Verlag.

McCarville P. and Crossey L. J. 1996. Post-impact hydrothermal alteration of the Manson impact structure. In *The Manson impact structure: Anatomy of an impact crater,* edited by Koeberl C. and Anderson R. R. Special Paper 302. Boulder: Geological Society of America. pp. 347–376.

McDonald I., Andreoli M. A. G., Hart R. J., and Tredoux M. 2001. Platinum-group elements in the Morokweng impact structure, South Africa: Evidence for the impact of a large ordinary chondrite projectile at the Jurassic-Cretaceous boundary. *Geochimica et Cosmochimica Acta* 65:299–309.

Naumov M. V. 1999. Hydrothermal-metasomatic mineralization. In *Deep drilling at Puchezh-Katuniki impact crater,* edited by Masaitis V. L. and Pevzner L. A. St. Petersburg: All-Russia Geological Research Institute. pp. 276–286. In Russian.

Naumov M. V. 2002. Impact-generated hydrothermal systems: Data from Popigai, Kara, and Puchezh-Katunki impact structures. In *Impacts in Precambrian shields,* edited by Plado J. and Pesonen L. J. Heidelberg: Springer Verlag. pp. 117–172.

Nesbitt H. W. and Young G. M. 1989. Formation and diagenesis of weathering profiles. *Journal of Geology* 97:129–147.

Plado J., Pesonen L. J., Puura V., and Suuroja K. 1996. Geophysical research on the Kärdla impact structure, Hiiumaa Island, Estonia. *Meteoritics & Planetary Science* 31:289–298.

Puura V. and Flodén T. 1997. The Baltic Sea drainage basin: A model of Cenozoic morphostructure reflecting the early Precambrian crustal pattern. In *Proceedings of the fourth marine geological conference: "The Baltic," Uppsala 1995,* edited by Cato I. and Klinberg F. Research Papers Ca 86. Uppsala: Sveriges Geologiska Undersökning. pp. 131–137.

Puura V. and Suuroja K. 1992. Ordovician impact crater at Kärdla, Hiiumaa Island, Estonia. *Tectonophysics* 216:143–156.

Puura V. A., Kala E. A., and Suuroja K. A. 1989. The structure of the Kärdla astrobleme (Hiiumaa Island, NW Estonia). *Meteoritika* 48:150–161. In Russian.

Puura V., Lindström M., Flodén T., Pipping F., Motuza G., Lehtinen M., Suuroja K., and Murnieks A. 1994. Structure and stratigraphy of meteorite craters in Fennoscandia and the Baltic region: A first outlook. Proceedings, Estonian Academy of Sciences. *Geology* 43:93–108.

Puura V., Amantov A., Tikhomirov S., and Laitakari I. 1996. Latest events affecting the Precambrian basement, Gulf of Finland, and surrounding areas. In *Explanation to the map of Precambrian basement of the Gulf of Finland and surrounding area 1:1 million,* edited by Koistinen T. Special Paper 21. Helsinki: Geological Survey of Finland. pp. 115–215.

Puura V., Kärki A., Kirs J., Kirsimäe K., Kleesment A., Konsa M., Niin M., Plado J., Suuroja K., and Suuroja S. 2000a. Impact-induced replacement of plagioclase by K-feldspar in granitoids and amphibolites at the Kärdla crater, Estonia. In *Impacts and the early Earth,* edited by Gilmour I. and Koeberl C. Heidelberg: Springer Verlag. pp. 415–445.

Puura V., Kärki A., Kirs J., Kirsimäe K., Konsa M., and Suuroja K. 2000b. Alteration of crater silicate rocks: Examples of dissimilar environments from Kärdla and Manson structures (abstract). In *Catastrophic events and mass extinctions: Impacts and beyond.* LPI Contribution 1053. Houston: Lunar and Planetary Institute. pp. 172–173.

Reimold W. U., Koeberl C., and Bishop J. 1994. Roter Kamm impact

crater, Namibia: Geochemistry of basement rocks and breccias. *Geochimica et Cosmochimica Acta* 58:2689–2710.
Ryder G. 2001. Mixing of target melt and projectile during impacts: Wet and dry target contrast (abstract). *Meteoritics & Planetary Science* 36:A180.
Stöckelmann D. and Reimold W. U. 1989. The HMX mixing calculation program. *Mathematical Geology* 21:853–860.
Suuroja K. 1996. Kärdla impaktkraatri teke ja areng. MSc thesis, Institute of Geology, University of Tartu, Tartu, Estonia.
Suuroja K., Suuroja S., All T., and Flodén T. 2002a. Kärdla (Hiiumaa Island, Estonia): The buried and well-preserved Ordovician marine impact structure. *Deep Sea Research II: Topical Studies in Oceanography* 49:1121–1144.
Suuroja K., Puura V., Kirs J., Niin M., and Põldvere A. 2002b. Geological setting of the Kärdla area. In *Soovälja (K-1) drill core,* edited by Põldvere A. Tallinn: Geological Survey of Estonia. pp. 6–10.
Taylor J. C. 1991. Computer programs for standardless quantitative analysis of minerals using the full powder diffraction profile. *Powder Diffraction* 6:2–9.
Taylor S. R. and McLennan S. M. 1985. *The continental crust: Its composition and evolution.* Oxford: Blackwell Scientific Publications. 312 p.
Török S. B. and van Grieken R. E. 1992. X-ray spectrometry. *Analytical Chemistry* 64:180–196.
Török S. B., Labar J., Injuk J., and van Grieken R. E. 1996. X-ray spectrometry. *Analytical Chemistry* 68:467–485.
Vishnevsky S. and Montanari A. 1999. Popigai impact structure (Arctic Siberia, Russia): Geology, petrology, geochemistry, and geochronology of glass-bearing impactites. In *Large meteorite impacts and planetary evolution II,* edited by Dressler B. O. and Sharpton V. L. Special Paper 339. Boulder: Geological Society of America. pp. 19–60.
Webby B. D. 1998. Steps toward a global standard for Ordovician stratigraphy. *Newsletter on Stratigraphy* 36:1–33.

APPENDIX

LITHOLOGIES AND PETROGRAPHY OF THE IMPACT-STRATIGRAPHIC UNITS

Kärdla Core Sequences K1 and K18: Description of Lithological Units

The lithologic units are classified and described according to their primary mineralogical composition and stratigraphic position. Thin section numbers refer to drill core samples analyzed chemically. Abbreviations of minerals are: Bt = biotite, Cal = calcite, Chl = chlorite, Hbl = hornblende, Hem = hematite, K-Fsp = K-feldspar, Mc = microcline, Or = orthoclase, Pl = plagioclase, Qtz = quartz.

Core K1 (300.0–815.2 m)

620.0–815.2 m Fractured Sub-Crater Basement: Impact-affected crystalline rocks, granites, and migmatites strongly prevailing over folded amphibolite bodies, fractured, locally crushed, and/or penetrated with minor breccia dikes, down to millimeters in width. The texture of the rock is massive, sporadically vesicular with concentric shock cracks around voids.

Granitoids: Qtz—Xenomorphic, with strong undulatory extinction, sporadically cataclastic, chipped in crushed zones. Mc—fresh crosshatched and with fissures of brecciation cutting the twinning. Pl—more or less replaced by earthy masses of a fine aggregate of Or. In relict Pl, polysynthetic twinning is partly preserved. Bt—slightly deformed and sporadically chloritized. Thin sections K1-8064/31, K1-8064/32, K1-7530/33, K1-7530/34.

Amphibolites: Hbl—In places, deformed and partly replaced by Chl, especially in brecciated zones. Pl—all grains are more or less replaced by a fine aggregate of K-Fsp, as in the granites. Thin sections K1-7810, K1-7734, K1-7660.

Breccia dikes: Veinlets of fine-grained aggregates in granitoids. Thin sections K1-8064/31, /32, K1-7530/33, /34.

589.0–620.0 m Strongly Fractured Sub-Crater Basement:

Strongly fractured granites with folded minor amphibolite bodies and widespread impact breccia dikes.

Granite: Qtz—as in the lowermost unit, sporadically more severely crushed and with sharp blocky extinction (K1-5960) but without PDFs. Mc—fresh crosshatched Mc. In brecciated zones, chipped and deformed (K1-6060). Pl—pseudomorphs of Or with relic polysynthetic twinning (K1-5990/1). Bt—deformed, locally chloritized. Thin sections K1-6060/35, K1-6060/36, K1-5990/1, K1-5990/2, K1-5960, K1-5895.

Amphibolite bodies are severely altered in zones of brecciation: Hbl is mechanically fragmented and replaced by Chl. Pl—largely replaced by K-Fsp aggregates in places with hematitic earthy masses. Thin sections K1-6030, K1-6018, K1-5970.

522.8–589.0 m Par-Autochthonous Breccia: Brecciated crystalline rocks, matrix-rich in lower part and clast-rich in upper part, derived mostly from granitic and, in fewer cases, from amphibolitic rocks. In places, very intensively folded Bt-gneiss (K1-5887) exists. Secondary calcite aggregates sporadically exist in matrix voids.

Most mineral clasts are Qtz. Besides sinuous, inclusions-trailed micro-fissures (K1-5425/A), one PDF system rarely was established. K-Fsp—Clasts are fresh but deformed crosshatched Mc without PDF. Pl is almost totally replaced by earthy K-Fsp and rusty hematite aggregate, in which rare relict areas with polysynthetic twinning occur. Bt shows kink bands and is partly chloritized. Few amphibolite clasts are represented as dark semi-opaque masses.

Breccia matrix consists of the same mineral clasts, crushed only to a finer grain size. Thin sections K1-5887, K1-5777, K1-5535, K1-5425/A, K1-5425/B, K1-5368, K1-5231.

471.0–522.8 m Allochthonous Breccia: Crystalline rock-derived matrix-supported breccia. Clasts are predominantly granite with minor amounts of amphibolite. Sporadically, matrix shows flow texture via kink-banded biotite flakes.

Clasts (mainly from granitoids): Qtz—1–2 (seldom up to 3; e.g., thin section K1-5073/2) systems of PDF. In addition, variably oriented rows of inclusions are seen. Inside Qtz, there are tiny patches with reduced refraction index—a possible occurrence of high-pressure Qtz polymorph (French 1998). In places, clasts with 1–2 PDF systems have been coalesced into one. Mc clasts are formed by relatively fresh but deformed, sporadically heavily kinked (K1-5075/2) crosshatched varieties. Pl shows relict polysynthetic twinning but is mainly replaced by submicroscopic Or aggregate containing voids with ripped edges. Sporadically up to 2 PDF systems is seen in Mc (K1-4947/1). Bt is kink-banded, sporadically containing patches of opaque or rusty masses. (K1-5073/1). Cal—dispersed aggregates and clasts in matrix (K1-5038/A)

Amphibolite clasts are replaced by chloritic masses, as in par-autochthonous breccia.

Matrix consists of the same clastic material crushed to a finer grain size. Thin sections K1-5162/1, K1-5162/2, K1-5159/1, K1-5159/2, K1-5075/1, K1-5075/2, K1-5073/1, K1-5073/2, K1-5032/B, K1-4947/1, K1-4947/2, K1-4945/1, K1-4945/2.

380.0–471.0 m Allochthonous Breccia: Sedimentary rock-derived breccia, clast-supported. Blocks and minor clasts are Cambrian sandstones and, locally, claystones; crystalline clasts are rare (see γ-ray log; Fig. 4).

356.0–380.0 m Allochthonous Breccia: Crystalline rock-derived breccia, predominately matrix-supported, with a granitic block in the middle. Sporadically, fragments of claystone are seen. Microscopic appearance, i.e., features and intensity of mineral deformation are exactly the same as in the unit 471.0–522.8 m.

Qtz—in clasts, 1 to 3 systems of PDFs are seen. Sinuous rows and zones of fluid inclusions are distributed in various directions. Often, clasts with different directions of PDFs are welded into one. Mc—Deformed, patchy crosshatched twinning is characteristic. Earthy and opaque inclusions are spreading partly along cleavage fractures, partly along sinuous crevasse-like fissures, partly in the form of irregular masses. In places, 1 PDF system is seen, diagonal in relation to crosshatching. Pl is replaced by earthy masses of Or. Bt shows kink-bands, is partly decomposed and chloritized. Cal occurs as dispersed aggregate in breccia groundmass and fissure-fillings, cutting clasts. Thin sections K1-3750/A, K1-3737/1, K1-3737/2, K1-3735/1, K1-3735/2.

300.0–356.0 m Allochthonous Breccia: Predominately sedimentary rock-derived, clast-supported breccia composed of blocks of Cambrian claystones with minor sandstones and blocks of Lower to Middle Ordovician limestone. Crystalline rocks clasts are rare in lower but more abundant in the upper part of the unit. Thin sections K1-3405/1, K1-3405/2, K1-3405/3, K1-3405/4, K1-3405/5.

300.0–~340 m Allochthonous Breccia: Locally abundant clasts of crystalline-derived breccias.

Mineral associations and clast population together with deformational features are exactly the same as those in the unit of 522.8–589.0 m. A grain of Qtz aggregate with PDFs in a crystalline breccia clast was found at a depth of 324 m. In Qtz of larger lithic clasts, no PDFs were found. Calcite in the form of veins and pore fillings is more abundant than in units 522.8-589.0 and 356.0-380.0 m. Thin sections K1-3255/A, K1-3255/B, K1-3240/A, K1-3240/B, K1-3240, K1-3240/1–5.

Core K18

400.0–431.4 m Sub-Crater Basement (Central Uplift):

Strongly fractured or brecciated crystalline rocks (migmatized biotite gneisses, microcline granites with folded amphibolite bodies) with impact breccia dikes. Mineral composition and deformational structures are the same as in the lowermost units of core K1. Rare carbonate veins and aggregates are seen in amphibolites.

In amphibolites, Pl is replaced by rusty masses of submicroscopic Or. Voids with irregular edges are visible. Hbl is replaced by pseudomorphs of Chl. Thin section K18-4000.

In granitoids, the fragmented Qtz grains and crosshatched Mc show mechanical deformation. Despite the large number of thin sections, PDFs of PFs in Qtz and Mc were not found, only submicroscopic inclusions filling various micro-fractures. Bt is slightly deformed, partly decomposed, and replaced with Chl. In places, kink-bands and alignment of Bt flakes around clasts is visible. Thin sections K18-4020/7, K18-4020/8, K18-4020/9, K18-4020/10, K18-4010/1, K18-4010/2, K18-4010/3, K18-4010/4, K18-4010/5, K18-4010/6, K18-4005/10, K18-4005/12-21, K18-4003.

356.0–400.0 m Allochthonous Breccia: This is the most thoroughly studied impact breccia unit in Kärdla. The mineral-textural fabric of this crystalline rock-derived, matrix-supported, fragmental breccia (K18-3830) follows.

Minerals and rock clasts, predominantly derived from granites, subordinately from amphibolites composed of Chl and Or with minor carbonate aggregates. Matrix—consists of welded microscopic-sub-microscopic clasts with massive, in places fluidal structure, partly with voids.

Qtz clasts, mostly 0.1–1 mm in size, very often show heavily patchy extinction with 2–3 systems of PDFs and

sinuous lines of fluid and opaque inclusions. K-Fsp exists either as fresh, crosshatched Mc (from basement granitoids) with refined, banded twin lamellae (with rare ladder textures), or as turbid sub-microscopically aggregates with rusty-pigmented Or patches replacing Mc. In large aggregates, clasts of Mc showing mosaicism, 1–2 systems of PDFs, and partly decorated with iron oxide earthy masses and beads were observed. Pl is replaced by sub-microscopic Or aggregates with some relict polysynthetic twinning. Bt flakes show kink- bands, partly chloritized, partly filled with hematitic ribbons in several directions. Thin sections K18-3997, K18-3984, K18-3975/1, K18-3975/2, K18-3964/1, K18-3964/2, K18-3960, K18-3960/A, K18-3960/B, K18-3960/28 - 30, K18-3930/25A, K18-3930/26, K18-3930/27, K18-3930/29, K18-3904/1, K18-3904/2, K18-3900/A, K18-3900/B, K18-3888, K18-3830, K18-3813/1, K18-3813/2, K18-3812/1, K18-3812/2, K18-3805/1, K18-3805/2, K18-3802/A, K18-3802/B, K18-3802/2, K18-3650, K18-3620, K18-3610.

292.7–356.0 m Allochthonous Breccia: Predominantly sedimentary rock-derived breccia composed of Cambrian sandstone and claystone blocks and clasts, with minor admixture of crystalline-derived clasts.

Crystalline-derived breccia mainly composed of granitic rocks dominates in the interval of 300–314 m or is presented as an admixture in the sedimentary breccia in the lower (314–340 m) and upper part (292.7–300 m) of the core. The sedimentary-rock-derived breccias are composed of Cambrian sandstones, claystones, and Ordovician limestones. Carbonate mineralization is abundant in the uppermost part of this unit. Thin sections K18-3010/A, K18-3010/B.

Crater Rim

Core Sections S8, F175, F241, F374, F376, F379, F380, F382, 413, 415

The crystalline core of the rim wall at Paluküla and Tubala is made of fractured and locally brecciated granites, granite-migmatites, and amphibolites, with impact breccia dikes and pockets. Locally in these cores, rich veins and pore fillings of calcite occur. In the groundmass of the rock, the replacement of primary Mc, Pl, and Hbl with above-described secondary aggregatic pseudomorphs is seen. No PDFs were observed in Qtz or other minerals. Thin sections F241-1673, F241-1330, F241-1063, F241-1053, F241-1004, F241-0967, F241-0795, F241-0574, F241-0546.

Core P11—depth interval 17–28 m, allochthonous breccia lens (pocket) on top of the crystalline core of the Paluküla rim. Crystalline-derived breccia is composed of granitic and amphibolitic rocks with fine clastic matrix and also with carbonate cement. Calcite veins cement brecciated granitoids in the uppermost part of crystalline rock sequence. In the clastic breccia matrix, partial relicts of Mc, Pl, Bt, and Hbl are visible. No PDFs were found in quartz or other minerals. Thin sections P11-0178/A–C, P11-0264/A–E, P11-0280/A–D.

Crystalline Basement Rocks from Outside the Crater

Samples were collected from drill cores located within a maximum radius of 25 km around the crater. Koppelmaa et al. (1996) made the petrographic characterization. Thin sections F361-3408, F361-2947, F361-2915, F361-2885, F364-3310, F364-3231, F364-3170, F364-3032, F364-3004, F364-2985, F364-2915.